

# Optimal Robust Precoders for Tracking the AoD and AoA of a mmWave Path

Nil Garcia, Henk Wymeersch, Dirk Slock

**Abstract**—Due to high penetration losses, millimeter wave channels are formed of few paths. Most channel estimation procedures exploit this property by sounding the channel in multiple directions and then identifying those yielding the largest power. Whether in initial access or tracking mode, the beams for sweeping the channel have maximum gain towards a small range of angles. These beams are heuristic in nature and may not lead the best estimation/tracking performance. In this paper, we investigate what are the optimal precoders for estimating the parameters of a single path, when prior knowledge is available, according to the well known Cramér-Rao lower bound. We use orthogonal matching pursuit (OMP) to compute such optimal precoders in a hybrid analog-digital architecture, but contrary to previous works which relied on approximations, we show how to apply OMP exactly for any type of array. To validate the theoretical results, the maximum likelihood estimators of the channel parameters are derived and their accuracy assessed.

## I. INTRODUCTION

MILLIMETER-WAVE (mmWave) communication is expected to be one of the key enablers of 5th generation cellular networks [1]. At such high frequencies exist large portions of unused bandwidth which have the potential to deliver multi-gigabit speeds [2]. Another well known advantage is that operating at higher carrier frequencies (30 GHz and above) allows for the compactification of large MIMO systems. Combining massive MIMO with beamforming will allow to compensate the large path loss at mmWave frequencies [3]. However, high-gain beamforming can only be performed after learning the channel.

In most types of environments, the mmWave channel is relatively sparse, in the sense that only a few multipath components have non-negligible energy at the receiver [4], [5]. This structure is leveraged in many techniques for performing quicker and/or finer channel estimation [6]–[10]. Typically, the output of initial channel estimation is a set of angle-of-departures (AoD), angle-of-arrivals (AoA) and channel gains of the individual paths. The mobility of the users and the variability of the environment [11], [12], makes it necessary to estimate the channel periodically. When in tracking mode, channel state information (CSI) is carried over to the next iteration, thus reducing the channel estimation overhead [13]–[16]. Another case where CSI is available is in location-aware communications [12], [17], [18]. The principle is that

prior knowledge on the user position (retrieved by some outer technology such as GPS) can also be used to enhance the channel estimation performance, for instance by narrowing the search space to a small range of angles such as in [19].

Common channel estimation procedures sweep the channel with highly directional beams at the transmitter and/or receiver [8], [20], [21]. By detecting the time at which the received power is the largest, the correct pair of beams can be identified and the AoD and/or AoA estimated for each path. While intuitive, such beams may not necessarily lead to the best achievable estimation accuracy. In this work, we seek to answer the question “what are the best precoders for tracking the parameters of a single path?”. For tractability and length purposes, we have limited the analysis to the case of a single path. Pure line-of-sight (LOS) mmWave communication is a simple solution which offers the added benefit of extremely low delay spread [22]. In addition, the angular and time information of the LOS path [23], [24] is an enabler for single-anchor high precision positioning [23], [24]. We assume that it is known, a priori, that the AoD and AoA lie within some narrow ranges such as it would happen when tracking the channel. Since the transmitter and receiver steer most of the energy towards this narrow ranges, it is safe to assume that we operate in an average to high SNR regime. Thus, a reasonable figure of merit is to use the Cramér-Rao bound (CRB) [23] on the AoD, AoA and channel gain. By employing tools from optimization and majorization, we are able to find the optimal precoders which minimize the CRB on these parameters. From a theoretical perspective, the proposed precoders provide new insights to the problem of beam design for channel estimation. From a practical perspective, while the optimization problem yielding the optimal precoders may not be suitable for real-time applications, these precoders may be useful for benchmarking purposes as they provide the best estimation performance. Moreover, its implementation in real estimation procedures is still feasible if they are computed offline and stored in the form of codebook.

The proposed precoders are obtained assuming fully digital arrays. However, due to their cost and power consumption, fully digital implementations of massive arrays are not viable. In order to benefit from the advantages of digital signal processing while maintaining a reasonable cost and consumption, quite a few hybrid analog-digital architectures have been proposed in the literature. Most of these architectures utilize discrete phase shifters, switches, low-resolution ADCs or even lenses [25]–[28] to shift some of the signal processing from the digital to the analog domain. In this work we assume the same architecture based on discrete phase shifters as in [6] and

N. Garcia and H. Wymeersch are with the Department of Signals and Systems, Chalmers University of Technology, Gothenburg, Sweden. D. Slock is with the Department of Communication Systems, EURECOM, Biot, France. This research was supported in part, by the EU HIGHTS project (High precision positioning for cooperative ITS applications) MG-3.5a-2014-636537, the VINNOVA COPPLAR project, funded under Strategic Vehicle Research and Innovation grant No. 2015-04849.

use the orthogonal matching pursuit (OMP) [29] algorithm to compute the phases of the analog phase shifters. While this approach to computing the analog and digital weights is not novel [30], it has not been used to its full potential. A common belief is that, for this problem, OMP cannot be computed exactly because the dictionary matrix grows exponentially with the number of antennas. To resolve this issue, previous works relied on some suboptimal computationally expensive variations of OMP [31], [32], or they simply reduced the dictionary in a heuristic manner [6], [33], [34]. In this work, we show that the operation of OMP which requires the full dictionary matrix can be computed exactly and efficiently without any approximation. Finally, to complement the design of the optimal precoders, we propose a new heuristic approach to the problem of designing analog combiners at the receiver. To validate the proposed precoders and combiners, maximum likelihood (ML) and low-complex estimators of the path parameters are developed and their performance is evaluated numerically.

## II. SIGNAL MODEL

Assume a transmitter (Tx) and a receiver (Rx) with  $N_{\text{Rx}}$  and  $N_{\text{Tx}}$  antennas, respectively. The transmitter sends  $M$  consecutive training sequences (or pilots) with each sequence precoded by the weigh vector  $\mathbf{f}_m$  and consisting of  $K$  symbols. Without loss of generalization assume the precoders are normalized to unit-norm. In arrays with large number of antennas, it is prohibitive to have a radio-frequency (RF) chain for each antenna. A common approach is to perform some sort of analog combining at the Rx in order to reduce the dimension of the received signals. Let  $N_{\text{Rx}}^{\text{RF}} (\leq N_{\text{Rx}})$  be the number of RF chains at the Rx, then assuming the same hybrid architecture than [6], the received snapshot for the  $k$ -th symbol of the  $m$ -th training sequence after analog combining and baseband conversion is

$$\mathbf{y}_{m,k} = \mathbf{W}^{\text{H}} (\mathbf{H} \mathbf{f}_m s_k + \mathbf{n}_{m,k}), \quad (1)$$

where  $\mathbf{W}$  is the combiner matrix of size  $N_{\text{Rx}} \times N_{\text{Rx}}^{\text{RF}}$ ,  $\mathbf{H}$  is the channel matrix, and  $\mathbf{n}_{m,k} \sim \mathcal{CN}(\mathbf{0}, \sigma^2 \mathbf{I}_{N_{\text{Tx}}})$  is white Gaussian noise. Let  $\mathbf{a}_{\text{Tx}}(\theta)$  and  $\mathbf{a}_{\text{Rx}}(\phi)$  be the array responses of the Tx and Rx, respectively. For the single path case, the MIMO channel matrix boils down to

$$\mathbf{H} = \alpha \mathbf{a}_{\text{Rx}}(\phi) \mathbf{a}_{\text{Tx}}^{\text{H}}(\theta), \quad (2)$$

where  $\alpha$ ,  $\phi$ ,  $\theta$ ,  $\tau$  are the channel gain, AoA, AoD and delay, respectively. Here, the implicit assumption is the bandwidth of the signal is much smaller than the carrier frequency, so that the array responses are independent of the frequency. Coherently aggregating the symbols of each training sequence results in

$$\mathbf{y}_m = \sum_{k=1}^K s_k^* \mathbf{y}_{m,k} = \mathbf{W}^{\text{H}} \left( \mathbf{H} \mathbf{f}_m + \sum_{k=1}^K s_k^* \mathbf{n}_{m,k} \right), \quad (3)$$

where  $\mathbf{s} = [s_1, \dots, s_K]$ . Finally, by stacking  $\mathbf{y}_1, \dots, \mathbf{y}_M$  as column vectors and dividing by  $\|\mathbf{s}\|_2$ , we reach the following matrix form for our signal model:

$$\mathbf{Y} = \frac{1}{\|\mathbf{s}\|_2} [\mathbf{y}_1 \ \cdots \ \mathbf{y}_M] = \|\mathbf{s}\|_2 \mathbf{W}^{\text{H}} \mathbf{H} \mathbf{F} + \mathbf{W}^{\text{H}} \mathbf{N} \quad (4)$$

where  $\mathbf{F} = [\mathbf{f}_1 \cdots \mathbf{f}_M]$  and the components of  $\mathbf{N}$  are i.i.d. Gaussian variables with variance  $\sigma^2$ . Contrary to many works [8]–[10], the spatial-temporal signal  $\mathbf{Y}$  is treated as our observations and no further baseband/digital combining is applied. Assuming  $\mathbf{W}$  is full rank, then the noise covariance is  $\mathbb{E} \mathbf{W}^{\text{H}} \mathbf{N} \mathbf{N}^{\text{H}} \mathbf{W} = \sigma^2 \mathbf{W}^{\text{H}} \mathbf{W}$ , and (4) can be whitened by a linear transformation

$$\tilde{\mathbf{Y}} = (\mathbf{W}^{\text{H}} \mathbf{W})^{-\frac{1}{2}} \mathbf{Y} = \|\mathbf{s}\|_2 \tilde{\mathbf{W}}^{\text{H}} \mathbf{H} \mathbf{F} + \tilde{\mathbf{N}}, \quad (5)$$

where

$$\tilde{\mathbf{W}} = \mathbf{W} (\mathbf{W}^{\text{H}} \mathbf{W})^{-\frac{1}{2}} \quad \text{and} \quad \tilde{\mathbf{N}} = \tilde{\mathbf{W}}^{\text{H}} \mathbf{N}. \quad (6)$$

It can be easily verified that  $\tilde{\mathbf{W}}$ 's columns are orthonormal, and consequently, the components of  $\tilde{\mathbf{N}}$  are white Gaussian random variables of variance  $\sigma^2$ . Hence, the result of applying an analog combiner is that the received signal across the array of antennas  $\mathbf{H} \mathbf{F}$  is projected onto the subspace of dimension  $N_{\text{Rx}}^{\text{RF}}$  spanned by the orthonormal columns of  $\tilde{\mathbf{W}}$ . In the next section our goal is to find the optimal precoders  $\mathbf{F}$  that minimize the Cramér-Rao bound on the variance of the AoD and/or AoA.

## III. OPTIMAL ROBUST PRECODERS

We are interested on the optimal precoders  $\mathbf{F}$  for estimating the AoD/AoA. When in tracking mode, a fair assumption is that prior estimates of the channel parameters are available. Assume that the AoD and AoA of the path of interest are known to be within some ranges of angles<sup>1</sup>, i.e.,  $\theta \in \mathcal{R}_{\text{Tx}}$  and  $\phi \in \mathcal{R}_{\text{Rx}}$ . If  $\mathcal{R}_{\text{Tx}}$  is a small enough region, it is reasonable that a certain beamforming gain will be achieved at the transmitter, and consequently, that we operate at a high-SNR regime (this assumption will be later verified by numerical analysis). The figure of merit of choice for optimizing the precoders is the Cramér-Rao bound (CRB) which is a lower-bound on the variance of any unbiased estimator. A well known property is that at high SNR, and under some mild conditions [35], the variance of the maximum likelihood estimator (MLE) is tight to the CRB. If  $\theta$  and  $\phi$  are the AoD and AoA, respectively, of the LOS path, then determining  $\theta$  yields the direction from the Tx to the Rx, and determining  $\phi$  provides the Rx's orientation with respect to the Tx. Thus, for naming purposes, we refer to the CRB on the  $\theta$  as direction error bound (DEB), and the CRB on  $\phi$  as orientation error bound (OEB). However, bear in mind that these error bounds and subsequent derivations also apply to any non-LOS path. From Appendix A, the direction error bound is

$$\text{var}(\hat{\theta}) \geq \text{DEB} = \left[ 2 \text{SNR} \left\| \tilde{\mathbf{W}}^{\text{H}} \mathbf{a}_{\text{Rx}}(\phi) \right\|_2^2 \left( \left\| \mathbf{F}^{\text{H}} \hat{\mathbf{a}}_{\text{Tx}}(\theta) \right\|_2^2 - \frac{|\mathbf{a}_{\text{Tx}}^{\text{H}}(\theta) \mathbf{F} \mathbf{F}^{\text{H}} \hat{\mathbf{a}}_{\text{Tx}}(\theta)|^2}{\left\| \mathbf{F}^{\text{H}} \mathbf{a}_{\text{Tx}}(\theta) \right\|_2^2} \right) \right]^{-1}, \quad (7)$$

<sup>1</sup>In practice, these ranges may correspond to confidence intervals.

and the orientation error bound is

$$\text{var}(\hat{\phi}) \geq \text{OEB} = \left[ 2 \text{SNR} \|\mathbf{F}^H \mathbf{a}_{\text{Tx}}(\theta)\|_2^2 \left( \left\| \widetilde{\mathbf{W}}^H \dot{\mathbf{a}}_{\text{Rx}}(\phi) \right\|_2^2 - \frac{|\mathbf{a}_{\text{Rx}}^H(\phi) \widetilde{\mathbf{W}} \widetilde{\mathbf{W}}^H \dot{\mathbf{a}}_{\text{Rx}}(\phi)|^2}{\left\| \widetilde{\mathbf{W}}^H \mathbf{a}_{\text{Rx}}(\phi) \right\|_2^2} \right) \right]^{-1}, \quad (8)$$

where

$$\text{SNR} = \frac{|\alpha|^2 \|\mathbf{s}\|_2^2}{\sigma^2}, \quad (9)$$

$\dot{\mathbf{a}}_{\text{Tx}}(\theta) \triangleq \frac{d\mathbf{a}_{\text{Tx}}(\theta)}{d\theta}$  and  $\dot{\mathbf{a}}_{\text{Rx}}(\phi) \triangleq \frac{d\mathbf{a}_{\text{Rx}}(\phi)}{d\phi}$ . Ideally, we would carry the optimization of the above lower-bounds over  $\mathbf{F}$  and  $\widetilde{\mathbf{W}}$  (or  $\mathbf{W}$ ), but this is hard because it requires that we impose pair-wise orthogonality and unit-norm among the columns of  $\widetilde{\mathbf{W}}$  (or involves matrix inversions when optimizing over  $\mathbf{W}$ ). Instead, we circumvent this problem by finding the optimal precoders  $\mathbf{F}$  given fixed combiners  $\mathbf{W}$ , and in Section IV-B, a solution to  $\widetilde{\mathbf{W}}$  is proposed which is independent of the choice of  $\mathbf{F}$ .

Both lower-bounds depend on the precoders  $\mathbf{F}$ , but also on the AoD  $\theta$  and AoA  $\phi$  which are unknown. Next, we propose a robust or min-max approach to the precoders design problem:

**Problem 1.** *Optimal robust precoders. Find the precoders that minimize the worst case DEB or OEB for all possible values of the AoD and AoA.*

$$\min_{\|\mathbf{f}_m\|_2=1, m=1, \dots, M} \max_{(\theta, \phi) \in \mathcal{R}_{\text{Tx}} \times \mathcal{R}_{\text{Rx}}} \max\{\text{DEB}, \text{OEB}\} \quad (10)$$

The dependence of the DEB and OEB on  $\theta$ ,  $\phi$  and  $\mathbf{F}$  has been omitted for notation clarity. Alternatively, if the only parameter of interest is the AoD, the robust precoders are the solution to:

**Problem 2.** *AoD-optimal robust precoders. Find the precoders that minimize the worst case DEB for all possible values of the AoD and AoA.*

$$\min_{\|\mathbf{f}_m\|_2=1, m=1, \dots, M} \max_{(\theta, \phi) \in \mathcal{R}_{\text{Tx}} \times \mathcal{R}_{\text{Rx}}} \text{DEB} \quad (11)$$

Conversely, if the only parameter of interest is the AoA, the robust precoders are obtained from:

**Problem 3.** *AoA-optimal robust precoders. Find the precoders that minimize the worst case OEB for all possible values of the AoD and AoA.*

$$\min_{\|\mathbf{f}_m\|_2=1, m=1, \dots, M} \max_{(\theta, \phi) \in \mathcal{R}_{\text{Tx}} \times \mathcal{R}_{\text{Rx}}} \text{OEB} \quad (12)$$

In the next section, we focus on deriving the solution to Problem 1 because the solutions to Problems 2 and 3 can be regarded as subcases. It will turn out that these problems can be reformulated as conic optimization programs, which is a subclass of convex problems.

## A. Convex Reformulation

Problem 1 is non-convex (with respect to  $\mathbf{F}$ ), and therefore, it is challenging to compute its global minimum efficiently. For a proof of non-convexity, note, for instance, that the OEB is concave because it is proportional to  $\|\mathbf{F}^H \mathbf{a}_{\text{Tx}}(\theta)\|_2^{-2}$ . An equivalent optimization problem (in the sense that yields the same solution) to Problem 1 is

$$\max_{\|\mathbf{f}_m\|_2=1, m=1, \dots, M} \min_{(\theta, \phi) \in \mathcal{R}_{\text{Tx}} \times \mathcal{R}_{\text{Rx}}} \min\{\text{DEB}^{-1}, \text{OEB}^{-1}\} \quad (13)$$

because  $f(x) = x^{-1}$  is a strictly decreasing function for  $x > 0$ . By introducing a slack variable  $t$ , the above problem can be expressed in the hypograph form:

$$\max_{\mathbf{F}, t} t \quad (14a)$$

$$\text{s.t.} \quad \min_{(\theta, \phi) \in \mathcal{R}_{\text{Tx}} \times \mathcal{R}_{\text{Rx}}} \text{DEB}^{-1} \geq t \quad (14b)$$

$$\min_{(\theta, \phi) \in \mathcal{R}_{\text{Tx}} \times \mathcal{R}_{\text{Rx}}} \text{OEB}^{-1} \geq t \quad (14c)$$

$$\|\mathbf{f}_m\|_2 = 1 \quad m = 1, \dots, L. \quad (14d)$$

The continuous set  $\mathcal{R}_{\text{Tx}} \times \mathcal{R}_{\text{Rx}}$  makes optimizing over constraints (14b)–(14c) challenging. Instead we approximate it by a grid  $\widetilde{\mathcal{R}}_{\text{Tx}} \times \widetilde{\mathcal{R}}_{\text{Rx}}$  such that

$$\widetilde{\mathcal{R}}_{\text{Tx}} = \{\vartheta^1, \dots, \vartheta^{S_{\text{Tx}}}\} \subset \mathcal{R}_{\text{Tx}} \quad (15)$$

$$\widetilde{\mathcal{R}}_{\text{Rx}} = \{\varphi^1, \dots, \varphi^{S_{\text{Rx}}}\} \subset \mathcal{R}_{\text{Rx}}. \quad (16)$$

Also for notation brevity, define

$$\begin{aligned} \mathbf{a}_{\text{Tx}}^i &\triangleq \mathbf{a}_{\text{Tx}}(\vartheta^i) & \dot{\mathbf{a}}_{\text{Tx}}^i &\triangleq \dot{\mathbf{a}}_{\text{Tx}}(\vartheta^i) \\ \mathbf{a}_{\text{Rx}}^q &\triangleq \mathbf{a}_{\text{Rx}}(\varphi^q) & \dot{\mathbf{a}}_{\text{Rx}}^q &\triangleq \dot{\mathbf{a}}_{\text{Rx}}(\varphi^q). \end{aligned} \quad (17)$$

Then, by replacing the continuous set by the grid, and since the DEB/OEB formulas (7)–(8) decouple into a part that depends only on  $\theta$  and another on  $\phi$ , the left side of (14b)–(14c) can be expressed as

$$\min_{(\theta, \phi) \in \mathcal{R}_{\text{Tx}} \times \mathcal{R}_{\text{Rx}}} \text{DEB}^{-1} = 2 \text{SNR} K_D \min_i \left( \left\| \mathbf{F}^H \dot{\mathbf{a}}_{\text{Tx}}^i \right\|_2^2 - \frac{|\mathbf{a}_{\text{Tx}}^{iH} \mathbf{F} \mathbf{F}^H \dot{\mathbf{a}}_{\text{Tx}}^i|^2}{\left\| \mathbf{F}^H \mathbf{a}_{\text{Tx}}^i \right\|_2^2} \right) \quad (18)$$

$$\min_{(\theta, \phi) \in \mathcal{R}_{\text{Tx}} \times \mathcal{R}_{\text{Rx}}} \text{OEB}^{-1} = 2 \text{SNR} K_O \min_i \left\| \mathbf{F}^H \mathbf{a}_{\text{Tx}}^i \right\|_2^2 \quad (19)$$

where  $K_D$  and  $K_O$  are the following constants (they do not depend on any of the optimizing variables)

$$K_D \triangleq \min_q \left\| \widetilde{\mathbf{W}}^H \mathbf{a}_{\text{Rx}}^q \right\|_2^2 \quad (20)$$

$$K_O \triangleq \min_q \left( \left\| \widetilde{\mathbf{W}}^H \dot{\mathbf{a}}_{\text{Rx}}^q \right\|_2^2 - \frac{|\mathbf{a}_{\text{Rx}}^{qH} \widetilde{\mathbf{W}} \widetilde{\mathbf{W}}^H \dot{\mathbf{a}}_{\text{Rx}}^q|^2}{\left\| \widetilde{\mathbf{W}}^H \mathbf{a}_{\text{Rx}}^q \right\|_2^2} \right). \quad (21)$$

Combining (14) with (18)–(19), results in

$$\max_{\mathbf{F}, t} t \quad (22a)$$

$$\text{s.t. } K_D \left( \|\mathbf{F}^H \dot{\mathbf{a}}_{\text{Tx}}^i\|_2^2 - \frac{|\mathbf{a}_{\text{Tx}}^{iH} \mathbf{F} \mathbf{F}^H \mathbf{a}_{\text{Tx}}^i|^2}{\|\mathbf{F}^H \mathbf{a}_{\text{Tx}}^i\|_2^2} \right) \geq t \quad (22b)$$

$$K_O \|\mathbf{F}^H \mathbf{a}_{\text{Tx}}^i\|_2^2 \geq t \quad (22c)$$

$$\|\mathbf{f}_m\|_2 = 1 \quad m = 1, \dots, M. \quad (22d)$$

for  $i = 1, \dots, S_{\text{Tx}}$ .

In order to transform (22) into a convex problem, two relaxations of the feasible set are proposed. If the solution to the newly relaxed problem is still within the original feasible set, then it is the optimum solution of the original problem. Perhaps surprisingly, this will indeed be our situation for the most part as explained in Section III-B. Let  $\text{diag}(\cdot)$  be the operator that returns the main diagonal of a matrix as a tall vector, let  $\text{Tr}(\cdot)$  be the matrix trace and let  $\mathbf{1}$  be the all-ones vector. Then, the constant energy constraint (22d) can also be expressed as  $\text{diag}(\mathbf{F}^H \mathbf{F}) = \mathbf{1}$ . The first proposed relaxation consists on replacing  $\text{diag}(\mathbf{F}^H \mathbf{F}) = \mathbf{1}$  by  $\text{Tr}(\mathbf{F} \mathbf{F}^H) (= \text{Tr}(\mathbf{F}^H \mathbf{F})) = M$ . For the second relaxation, first, we make the variable change

$$\mathbf{X} = \mathbf{F} \mathbf{F}^H, \quad \text{rank } \mathbf{X} \leq M, \quad \mathbf{X} \succcurlyeq 0, \quad (23)$$

where ‘ $\succcurlyeq$ ’ denotes positive semidefinite matrix. This is a valid variable change because  $\mathbf{F}$  can always be recovered from  $\mathbf{X}$  by performing, for instance, a Cholesky decomposition. The second relaxation consists in dropping the rank constraint. Thus, the new optimization problem after including the two relaxations and performing the variable change is

$$\max_{\mathbf{X}, t} t \quad (24a)$$

$$\text{s.t. } K_D \left( \dot{\mathbf{a}}_{\text{Tx}}^{iH} \mathbf{X} \dot{\mathbf{a}}_{\text{Tx}}^i - \frac{|\mathbf{a}_{\text{Tx}}^{iH} \mathbf{X} \mathbf{a}_{\text{Tx}}^i|^2}{\mathbf{a}_{\text{Tx}}^{iH} \mathbf{X} \mathbf{a}_{\text{Tx}}^i} \right) \geq t \quad (24b)$$

$$K_O \mathbf{a}_{\text{Tx}}^{iH} \mathbf{X} \mathbf{a}_{\text{Tx}}^i \geq t \quad (24c)$$

$$\text{Tr } \mathbf{X} = M \quad (24d)$$

$$\mathbf{X} \succcurlyeq 0 \quad (24e)$$

for  $i = 1, \dots, S_{\text{Tx}}$ . Constraint (24b) can be cast (see Section 2.3. in [36]) as a second order cone (25b),

$$\max_{\mathbf{X}, t} t \quad (25a)$$

$$\left\| \left( \dot{\mathbf{a}}_{\text{Tx}}^{iH} \mathbf{X} \dot{\mathbf{a}}_{\text{Tx}}^i - \frac{2\mathbf{a}_{\text{Tx}}^{iH} \mathbf{X} \mathbf{a}_{\text{Tx}}^i}{K_D} - \mathbf{a}_{\text{Tx}}^{iH} \mathbf{X} \mathbf{a}_{\text{Tx}}^i \right) \right\|_2 \leq \dot{\mathbf{a}}_{\text{Tx}}^{iH} \mathbf{X} \dot{\mathbf{a}}_{\text{Tx}}^i - \frac{t}{K_D} + \mathbf{a}_{\text{Tx}}^{iH} \mathbf{X} \mathbf{a}_{\text{Tx}}^i \quad (25b)$$

$$K_O \mathbf{a}_{\text{Tx}}^{iH} \mathbf{X} \mathbf{a}_{\text{Tx}}^i \geq t \quad (25c)$$

$$\text{Tr } \mathbf{X} = M \quad (25d)$$

$$\mathbf{X} \succcurlyeq 0, \quad (25e)$$

where  $i = 1, \dots, S_{\text{Tx}}$ . Problem (25) is a conic program [37] (and consequently convex) because it is composed of linear constraints, second order cones (25b) and a positive semidefinite cone (25e). An advantage of having reformulated

our problem as a conic program is that they are well known in the literature and very efficient solvers exist [38], [39].

For the solution to Problem 2 simply solve the same problem (25) without constraint (25c). By deleting (25c) and performing the variable change  $\frac{t}{K_D} \leftarrow t$ , constants  $K_O$  and  $K_D$  disappear, making the optimization problem independent of the receiver’s array response. To obtain the solution to Problem 3 delete (25b), and following the same reasoning, the optimization problem also becomes independent of the receiver’s array response.

*Remark:* When the Tx (or the Rx) is equipped with a ULA, the DEB (or OEB) tends to infinite at the endfire. This is because, for the ULA case, there exists no unbiased AoD (or AoA) estimator when the endfire is part of the search space. For an in-depth explanation of this phenomenon see [40]. However, as done in many works [41], this problem can be circumvented if one defines a new parameter ‘spatial frequency’  $\omega = \frac{\cos(\theta)}{2}$  (or  $\omega = \frac{\cos(\phi)}{2}$ ) assuming the ULA is aligned along the  $x$ -axis, and treats  $\omega$  as the unknown parameter instead of  $\theta$  (or  $\phi$ ).

## B. Recovery of the Precoders

We abuse the notation and call  $\mathbf{X}$  the global maximizer of (25) (not the optimizing variable). In the previous section, Problem 1 was transformed into a convex problem (25) by performing a grid approximation (14)–(22) and by relaxing the feasible set (22)–(25). The grid approximation is sufficiently exact if dense enough. On the other hand, it remains to see if the relaxed problem (25) has the same solution as (22). In other words, we need to check if there exists a set of precoders  $\mathbf{F}$  that reverts the variable change (23) and lie in the original feasible set, i.e.,

$$\text{C1) } \text{rank } \mathbf{X} \leq M$$

$$\text{C2) } \text{diag}(\mathbf{F}^H \mathbf{F}) = \mathbf{1}$$

Condition C1 implies that the rank of  $\mathbf{X}$  must be less than or equal to the number of training sequences. Interestingly, as shown in Section VI-A,  $\mathbf{X}$  tends to be low-rank due to the *sparsifying* constraint (25d). That trace constraint induces low-rank solutions is well known in the compressive sensing literature [42], [43]. Consequently, if  $M$  can be chosen sufficiently large, then C1 will be satisfied. The remainder of this section is devoted to finding if C2 is satisfied provided that C1 is satisfied.

Let the eigendecomposition of  $\mathbf{X}$  and the singular value decomposition (SVD) of  $\mathbf{F}$ , respectively, be

$$\mathbf{F} = \mathbf{U} \mathbf{\Sigma} \mathbf{V}^H \quad (26)$$

$$\mathbf{X} = \mathbf{Q} \mathbf{\Lambda} \mathbf{Q}^H, \quad (27)$$

where  $\mathbf{U}$ ,  $\mathbf{V}$  are  $\mathbf{Q}$  are unitary matrices, and define  $R \triangleq \text{rank}(\mathbf{X}) \leq M$ . We can use the *compact* eigendecomposition of  $\mathbf{X}$ , whereby  $\mathbf{Q} = [\mathbf{q}_1 \cdots \mathbf{q}_R]$  and  $\mathbf{\Lambda} = \text{Diag}(\lambda_1 \cdots \lambda_R)$ , include only the  $R$  eigenvectors associated to the  $R$  non-zero eigenvalues sorted in non-increasing order. The variable change (23) exists if, and only if,  $\text{rank}(\mathbf{F}) = R$ . Thus, if we limit ourselves to the study of matrices  $\mathbf{F}$  with rank  $R$ , then  $\mathbf{F}$  can also be represented by using the *compact* SVD, whereby

$\mathbf{U} = [\mathbf{u}_1 \cdots \mathbf{u}_R]$ ,  $\mathbf{V} = [\mathbf{v}_1 \cdots \mathbf{v}_R]$  and  $\mathbf{\Sigma} = \text{Diag}(\mu_1 \cdots \mu_R)$  include only the  $R$  singular left and right vectors associated to the  $R$  non-zero singular values ordered in non-increasing order. From the definition of the SVD, the left singular vectors and the singular values of  $\mathbf{F}$  are, respectively, the eigenvectors and square roots of the eigenvalues of  $\mathbf{F}\mathbf{F}^H$ , but  $\mathbf{F}\mathbf{F}^H = \mathbf{X}$  precisely. Therefore,

$$\mathbf{u}_r = \mathbf{q}_r \quad (28)$$

$$\mu_r = \sqrt{\lambda_r}, \quad (29)$$

for  $r = 1, \dots, R$ . Summarizing if  $\mathbf{F}$  exists, its left singular vectors and singular values are given by (28) and (29). Next, it remains to see if such matrix  $\mathbf{F}$  can satisfy condition C2.

By replacing  $\mathbf{F}$  with its SVD, condition C2 transforms into

$$\text{diag}(\mathbf{V}\mathbf{\Sigma}^2\mathbf{V}^H) = \mathbf{1}. \quad (30)$$

However,  $\mathbf{\Sigma}^2$  is a diagonal matrix whose entries are prescribed by (29), and therefore, the only degrees of freedom left are the entries of the unitary matrix  $\mathbf{V}$ . Notice that  $\mathbf{V}\mathbf{\Sigma}^2\mathbf{V}^H$  may be regarded as the eigendecomposition of a matrix whose eigenvector matrix is  $\mathbf{V}$  and whose eigenvalues are  $\mu_1^2 \dots, \mu_R^2$ . Consequently, condition (30) is equivalent to the existence of a matrix with prescribed eigenvalues  $\mu_1^2 \dots, \mu_R^2$  and main diagonal filled with 1's. Fortunately, the Schur-Horn theorem (see Theorem B.1. in [44], p. 218) states that such matrix exists if, and only if, the eigenvalues majorize the diagonal values, i.e.,

$$\sum_{m=1}^{m'} \mu_m^2 \left( = \sum_{m=1}^{m'} \lambda_m \right) \geq \sum_{m=1}^{m'} d_m \quad m' = 1, \dots, M, \quad (31)$$

where  $d_m$  are the diagonal values in non-increasing order, and in our particular case  $d_m = 1$  for all  $m$ . As proven next, this condition is always satisfied for the particular case that diagonal values are all equal. Define the average of the first  $m'$  eigenvalues:  $S_{m'} \triangleq \sum_{m=1}^{m'} \lambda_m / m'$ . Note that (31) is equivalent to  $\sum_{m=1}^{m'} \lambda_m \geq m'$  for  $m' = 1, \dots, M$ , and by dividing both sides of the inequality by  $m'$ , the condition turns into  $S_{m'} \geq S_M$ . Since the the lambdas are sorted in non-decreasing order, it is straightforward that the condition holds unconditionally.

We have proven that there exists a matrix  $\mathbf{F}$  satisfying C2 if C1 is true, next, a method for recovering the precoders is provided. The left singular vectors and singular values of  $\mathbf{F}$  are retrieved by (28) and (29), respectively. For the right singular vectors, the Bendel-Mickey algorithm [45], [46] can find a matrix with prescribed eigenvalues and constant main diagonal. Thus, we find a matrix  $\mathbf{B}$  with prescribed eigenvalues  $\lambda_1, \dots, \lambda_R$  and constant main diagonal using the Bendel-Mickey algorithm, and then, its eigenvectors are the singular right vectors of  $\mathbf{F}$ . For the case that C1 is not satisfied and the number of training sequences  $M$  cannot be increased, then a suboptimal  $\mathbf{F}$  can still be obtained by performing a rank  $M$  approximation of  $\mathbf{X}$ . A simple approximation consists in keeping only the  $M$  largest eigenvalues and the corresponding eigenvectors of  $\mathbf{X}$ , and to rescale such matrix in order to satisfy C2. Algorithm 1 summarizes the steps for retrieving

the precoders. In general, this algorithm returns a different precoder every time it is executed even for the same matrix  $\mathbf{X}$  because the solution provided by the Bendel-Mickey algorithm is random.

---

#### Algorithm 1 Retrieval of the precoders $\mathbf{F}$ from $\mathbf{X}$

---

**inputs:**  $\mathbf{X}, M$

**outputs:**  $\mathbf{F}$

- 1: **if**  $\text{rank}(\mathbf{X}) > M$  **then**
  - 2:   compute  $M$ -rank approximation of  $\mathbf{X}$  and scale it so that its trace equals  $M$
  - 3: **end if**
  - 4: compute the eigendecomposition of  $\mathbf{X}$  and denote  $\mathbf{q}_1, \dots, \mathbf{q}_R$  the eigenvectors associated to the  $R \triangleq \text{rank}(\mathbf{X})$  non-zero eigenvalues  $\lambda_1, \dots, \lambda_R$  sorted in descending order, respectively
  - 5: find a matrix  $\mathbf{B}$  of size  $M \times M$  with all diagonal values equal to 1 and eigenvalues  $\lambda_1, \dots, \lambda_R$  by the Bendel-Mickey algorithm<sup>2</sup> [45], [46]
  - 6: compute the eigendecomposition of  $\mathbf{B}$  and let  $\mathbf{v}_1, \dots, \mathbf{v}_R$  be its eigenvectors associated to the  $R$  non-zero eigenvalues  $\lambda_1, \dots, \lambda_R$ , respectively
  - 7: set  $\mathbf{F} = [\mathbf{q}_1 \cdots \mathbf{q}_R] \text{Diag}(\sqrt{\lambda_1} \cdots \sqrt{\lambda_R}) [\mathbf{v}_1 \cdots \mathbf{v}_R]^H$
- 

*Remark:* If the Tx uses different power to transmit the  $M$  training sequences, then (31) may not always be satisfied, and therefore, the optimum  $\mathbf{F}$  may not be retrieved by solving problem (25). However, if (31) is satisfied (where  $d_m$  is the energy of the  $m$ -th training sequence), then the optimum  $\mathbf{F}$  may still be retrieved using the same Algorithm 1 while replacing the Bendel-Mickey algorithm by the one in [47]. Thus, access to the optimum solution will depend on the choice of powers and the eigenvalues of  $\mathbf{X}$ .

*Examples:* Define the antenna gain function at the Tx as

$$g(\theta, \mathbf{f}_m) = |\mathbf{f}_m^H \mathbf{a}_{\text{Tx}}(\theta)|, \quad (32)$$

and the total gain (which is the equivalent gain at the receiver if the energy of the  $M$  training sequences is coherently combined) as

$$g_{\text{T}}(\theta) = \left( \sum_{m=1}^M |\mathbf{f}_m^H \mathbf{a}_{\text{Tx}}(\theta)|^2 \right)^{-\frac{1}{2}}. \quad (33)$$

As an example, Fig. 1 plots the beampatterns (gain vs. azimuth) of the optimal precoders obtained by solving Problems 1–3. The AoD-optimal precoders result in beampatterns (see Fig. 1b) with many ripples, whereas the AoA-optimal precoders try to deliver the highest gain (Fig. 1c), and the (AoD-AoA)-optimal precoders are somewhere in between (see Fig. 1a). The reason for this is that different AoDs result in different transmit power and phase for each precoder  $m$ . By looking at how this power and phase changes across the  $M$  training sequences, the Rx is able to estimate the AoD. Thus, in order to increase the accuracy on the AoD, the Tx must use precoders whose beampatterns vary quickly as a function

<sup>2</sup>Code available in Matlab R2015b by the name `gallery('randcorr', arg)`.

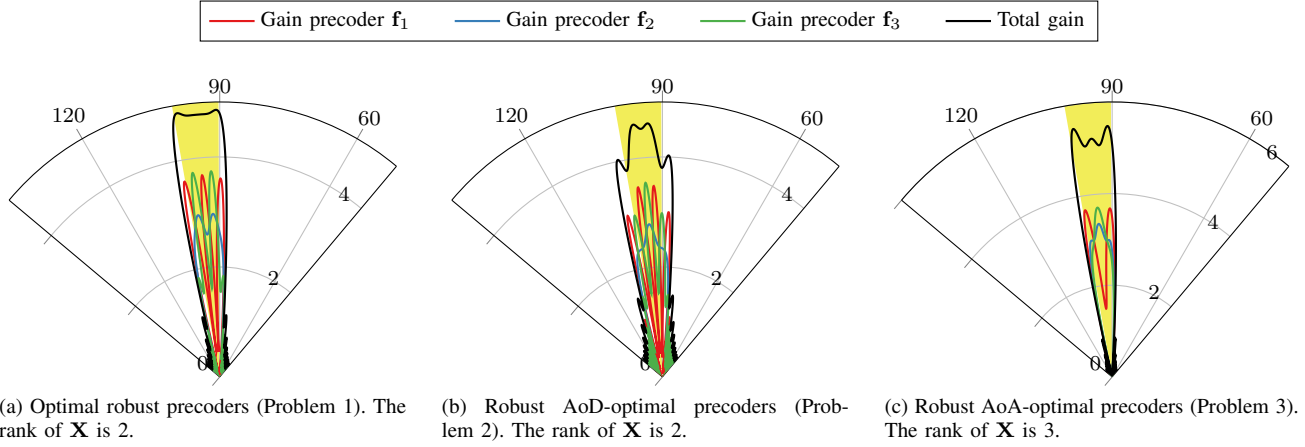


Fig. 1. Antenna gain of the precoders vs. azimuth for all  $M$  precoders. The Tx and Rx are equipped with 30-antenna half-wavelength inter antenna spacing ULAs. The number of training sequences is  $M = 3$ . The AoD (same for the AoA for simplicity) is known a priori to lie in the range  $[90^\circ, 100^\circ]$ , indicated by the yellow shaded area. According to Section III-B, the optimality of these precoders is ensured because for all cases  $M \geq \text{rank } \mathbf{X}$ .

of the AoD. On the other hand AoA estimation is performed by comparing the spatial signature of the received signal at the Rx. The only repercussion the Tx has on the received signal across the Rx antennas is in terms of power. Thus, the AoA accuracy is improved by choosing precoders that transmit maximum power, i.e., maximize the gain. Interestingly, these beampatterns do not resemble “sector beams”, whose gain is large for a small range of angles and low for all other, which are commonly used for estimating AoDs and AoAs [8], [21], [48].

### C. Additional Constraints

The proposed set of robust precoders (10)–(12) are purely oriented to minimizing the CRB of the AoD and/or AoA. However, in practice some additional constraints may be desired, such as null steering towards certain directions in order to mitigate multi user interference or cancel certain paths. Next, it is shown how some of these constraints can easily be added to the original optimization problems.

1) *Identifiability of the AoD and AoA*: A necessary condition for correctly estimating the AoD and/or AoA is that they are identifiable. The AoA and AoD are identifiable provided that the received signals (5) in absence of noise are different

$$\alpha \mathbf{W}^H \mathbf{a}_{\text{Rx}}(\phi) \mathbf{a}_{\text{Tx}}^H(\theta) \mathbf{F} \neq \alpha' \mathbf{W}^H \mathbf{a}_{\text{Rx}}(\phi') \mathbf{a}_{\text{Tx}}^H(\theta') \mathbf{F}, \quad (34)$$

for all possible  $\theta \neq \theta'$  in  $\mathcal{R}_{\text{Tx}}$ ,  $\phi \neq \phi'$  in  $\mathcal{R}_{\text{Rx}}$ , or  $\alpha \neq \alpha'$ . Since the signals are rank 1 matrices, the condition decouples into pair-wise linear independence between steering vectors at the Rx and Tx:

$$\beta \mathbf{W}^H \mathbf{a}_{\text{Rx}}(\phi) \neq \beta' \mathbf{W}^H \mathbf{a}_{\text{Rx}}(\phi') \quad (35)$$

$$\gamma \mathbf{F}^H \mathbf{a}_{\text{Tx}}(\theta) \neq \gamma' \mathbf{F}^H \mathbf{a}_{\text{Tx}}(\theta') \quad (36)$$

for all complex  $\beta, \beta', \gamma, \gamma'$  different than zero. Condition (35) depends on the Rx array response and the combiner  $\mathbf{W}$ . For the particular case of a fully digital Rx ( $\mathbf{W} = \mathbf{I}_{N_{\text{Rx}}}$ ), this condition is in general satisfied for most common types of arrays [49], [50]. Our focus is in the design of the precoders, thus we turn to condition (36). This condition depends on

the Tx array response and on the precoders  $\mathbf{F}$ . Thus, careful attention needs to be put on the precoders to avoid creating ambiguities. Pair-wise linear independence (36) is equivalent to  $|\mathbf{a}_{\text{Tx}}^H(\theta) \mathbf{F} \mathbf{F}^H \mathbf{a}_{\text{Tx}}(\theta')|^2 / \|\mathbf{F}^H \mathbf{a}_{\text{Tx}}(\theta)\|_2^2 \|\mathbf{F}^H \mathbf{a}_{\text{Tx}}(\theta')\|_2^2 < 1$ . Thus, in order to ensure that the AoD is identifiable we propose to add the following constraints to problem (25):

$$\frac{|\mathbf{a}_{\text{Tx}}^H(\vartheta^i) \mathbf{F} \mathbf{F}^H \mathbf{a}_{\text{Tx}}(\vartheta^{i'})|^2}{\|\mathbf{F}^H \mathbf{a}_{\text{Tx}}(\vartheta^i)\|_2^2 \|\mathbf{F}^H \mathbf{a}_{\text{Tx}}(\vartheta^{i'})\|_2^2} < \rho \quad (37)$$

for all  $i, i'$  such that  $\vartheta^i - \vartheta^{i'} > D \pmod{360^\circ}$ , where  $0 \leq \rho < 1$  and  $D$  is the angular resolution of the array<sup>3</sup>. By performing the variable change  $\mathbf{X} = \mathbf{F} \mathbf{F}^H$  and some algebraic manipulations [36], (37) can be expressed as a second order cone (convex constraint):

$$\left\| \begin{pmatrix} 2 \mathbf{a}_{\text{Tx}}^{iH} \mathbf{X} \mathbf{a}_{\text{Tx}}^{i'} \\ \sqrt{\rho} \mathbf{a}_{\text{Tx}}^{iH} \mathbf{X} \mathbf{a}_{\text{Tx}}^i - \sqrt{\rho} \mathbf{a}_{\text{Tx}}^{i'H} \mathbf{X} \mathbf{a}_{\text{Tx}}^{i'} \end{pmatrix} \right\|_2 \leq \sqrt{\rho} \mathbf{a}_{\text{Tx}}^{iH} \mathbf{X} \mathbf{a}_{\text{Tx}}^i + \sqrt{\rho} \mathbf{a}_{\text{Tx}}^{i'H} \mathbf{X} \mathbf{a}_{\text{Tx}}^{i'}, \quad (38)$$

where the shortened notation (17) was used.

2) *Out-of-Range Attenuation*: To avoid multi user interference or to null-steer towards the AoDs of other paths that are not of interest, a practical approach is to create beampatterns with low attenuation in those directions. From Fig. 1, it is clear that there is some energy radiated in directions out of the prior range  $\mathcal{R}_{\text{Tx}}$ . Let  $\{\pi^q\}_{q=1}^{S_a}$  be the AoDs for which we wish to enforce a lower transmitting power. The total transmitted energy in direction  $\pi^q$  over the  $M$  training sequences is  $\|\mathbf{F}^H \mathbf{a}_{\text{Tx}}(\pi^q)\|_2^2$ . Let  $A_q < 1$  be the desired attenuation factor, then, we propose to add the following constraint to problem (25),

$$\|\mathbf{F}^H \mathbf{a}_{\text{Tx}}(\pi^q)\|_2^2 \leq A_q \|\mathbf{F}^H \mathbf{a}_{\text{Tx}}(\vartheta^i)\|_2^2 \quad (39)$$

<sup>3</sup>The resolution of the array is typically related to the antenna aperture and is different for each array configuration. In practice, one could start with an approximate value and then tweak this parameter. For instance, for an  $N$ -antennas half-wavelength inter-antenna spaced UCA, the angle resolution has been checked numerically to be well approximately by  $1.6 \sin(\pi/N)$  [radians].

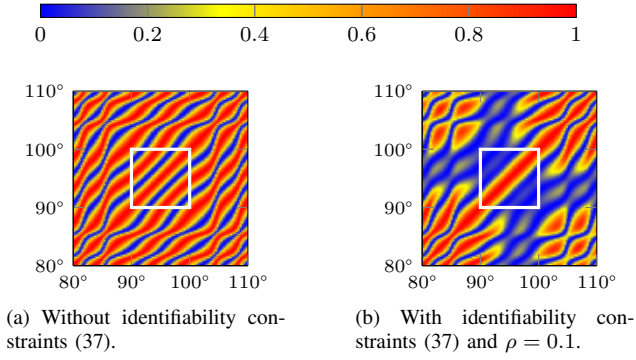


Fig. 2. Colormap of left hand side of (37) versus  $\theta$  and  $\theta'$  when employing optimal beams. The Tx and the Rx have, each, a 30-antennas UCA. The number of training sequences  $M = 4$  and the rank of  $\mathbf{X}$  is 4. It is known a priori that the AoD lies in the interval  $\mathcal{R}_{\text{Tx}} = [90^\circ, 100^\circ]$ . The white square indicates the region  $\mathcal{R}_{\text{Tx}} \times \mathcal{R}_{\text{Tx}}$ .

for  $q = 1, \dots, S_a$  and  $i = 1, \dots, S_{\text{Tx}}$ , which can be transformed to linear constraints after performing the variable change  $\mathbf{X} = \mathbf{F}\mathbf{F}^H$ ,

$$\mathbf{a}_{\text{Tx}}^H(\pi^q) \mathbf{X} \mathbf{a}_{\text{Tx}}(\pi^q) \leq A_q \mathbf{a}_{\text{Tx}}^H(\vartheta^i) \mathbf{X} \mathbf{a}_{\text{Tx}}(\vartheta^i). \quad (40)$$

These  $S_a S_{\text{Tx}}$  constraints can be reduced to  $S_a + S_{\text{Tx}}$  by incorporating a dummy variable  $z$ ,

$$\mathbf{a}_{\text{Tx}}^H(\pi^q) \mathbf{X} \mathbf{a}_{\text{Tx}}(\pi^q) \leq A_q z \quad q = 1, \dots, S_a \quad (41)$$

$$\mathbf{a}_{\text{Tx}}^H(\vartheta^i) \mathbf{X} \mathbf{a}_{\text{Tx}}(\vartheta^i) \geq z \quad i = 1, \dots, S_{\text{Tx}}. \quad (42)$$

*Examples:* Fig. 2 plots the left hand side of (37) when the precoders are obtained with or without the identifiability constraint. Ideally, only the anti-diagonal across the white square should be red as is the case in the right figure. The left figure, has two red stripes, and therefore, there are pairs of AoDs within the range  $\mathcal{R}_{\text{Tx}}$  which result in the same signals, and consequently are not identifiable even in the absence of noise.

In Fig. 3 two sets of optimal robust precoders are generated. The first set of precoders has no constraint on the total gain (33) towards directions outside of the range of interest  $\mathcal{R}_{\text{Tx}}$ . The second set of precoders imposes a 20 dB attenuation in the range  $[150^\circ, 220^\circ]$  and a null at  $310^\circ$ . Note that the total gain within the range is virtually the same for both sets of precoders.

#### IV. HYBRID ANALOG-DIGITAL DESIGN

According to [1], *digital beamforming provides a higher degree of freedom and offers better performance at the expense of increased complexity and cost, whereas analog beamforming, on the other hand, is a simple and effective method of generating high beamforming gains from a large number of antennas but less flexible.* This trade-off between the performance of digital and simplicity of analog architectures has sparked a strong interest in hybrid analog-digital beamforming architectures that get the best of both worlds.

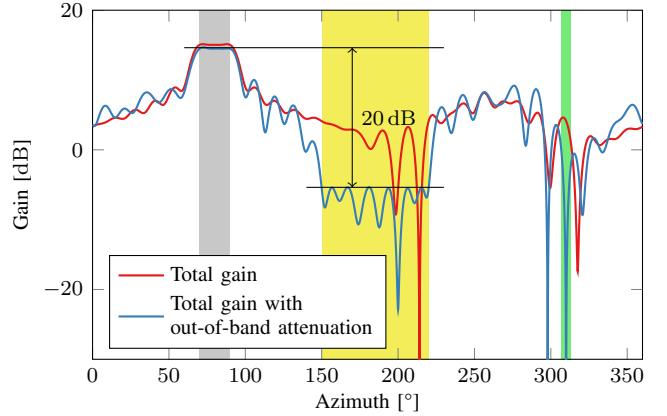


Fig. 3. Total gain (33) of the optimal robust precoders vs. azimuth. The Tx and Rx are equipped with 30-antenna half-wavelength inter antenna spacing UCAs. The number of training sequences is  $M = 3$  and the rank  $\mathbf{X}$  is 2, ensuring these are the optimal precoders. The AoD (same for the AoA for simplicity) is known a priori to lie in the range  $[70^\circ, 90^\circ]$ , indicated by the grey shaded bin. Two different sets of precoders are used. First set is the optimum solution to Problem 1. The second set is the optimum solution to Problem 1 while imposing a 20 dB attenuation in the range  $[150^\circ, 220^\circ]$  indicated by the yellow shaded bin, and a null at  $310^\circ$  indicated by the green shaded bin.

#### A. Signal Model for Hybrid Arrays

Many hybrid architectures have been proposed in the literature that combine analog and digital signal processing. Among the many proposed hybrid architectures, in this paper we consider the same in [6]. The analog frontend is composed of phase shifters of finite resolution, signal splitters and combiners. The number of bits  $B$  used to control the phase shifter determines the number of possible discrete phase shifts  $Q = 2^B$ :

$$\mathcal{X} = \left\{ 1, e^{\frac{j2\pi}{Q}}, \dots, e^{\frac{j2\pi(Q-1)}{Q}} \right\}. \quad (43)$$

Each RF chain splits/combiners the signal of all antennas after phase shifting. Both the Tx and the Rx are assumed to have the same hybrid architecture, but possibly different number of RF chains and bits to control the phase shifters. Let  $N_{\text{Tx}}^{\text{RF}}$  and  $N_{\text{Rx}}^{\text{RF}}$  be the number of RF chains at the Tx and Rx, respectively. Then, mathematically, the hybrid architecture at the Tx can be modeled as

$$\mathbf{f}_m = \mathbf{F}_m^{\text{RF}} \mathbf{f}_m^{\text{BB}}, \quad (44)$$

where  $\mathbf{F}_m^{\text{RF}} \in \mathcal{X}^{N_{\text{Tx}} \times N_{\text{Tx}}^{\text{RF}}}$  and  $\mathbf{f}_m \in \mathbb{C}^{N_{\text{Tx}}^{\text{RF}} \times 1}$ . RF and BB are short for radio-frequency (analog) and base-band (digital). At the Rx, the weights of the analog combiners (4) need to be elements of (43), i.e.,  $\mathbf{W} \in \mathcal{X}^{N_{\text{Rx}} \times N_{\text{Rx}}^{\text{RF}}}$ .

#### B. Precoders Design

The hybrid precoders are modeled by equation (44). Ideally, Problems 1 to 3 should be solved globally by making the substitution  $\mathbf{f}_m = \mathbf{F}_m^{\text{RF}} \mathbf{f}_m^{\text{BB}}$  and optimizing over  $\mathbf{F}_m^{\text{RF}}$  and  $\mathbf{f}_m^{\text{BB}}$  for all  $m$ . However, this approach would yield a large-scale optimization problem with discrete and continuous variables for which the global solution cannot be computed efficiently. From here on, we abuse the notation and denote by  $\{\mathbf{f}_m\}_{m=1}^M$ , the optimal fully digital precoders obtained by following the

procedure in Section III. An alternative heuristic approach is to find the closest hybrid precoders, in a least squares sense, to the optimal fully digital precoders,

$$\min_{\substack{\mathbf{F}_m^{\text{RF}} \in \mathcal{X}^{N_{\text{Tx}} \times N_{\text{Tx}}^{\text{RF}}} \\ \mathbf{f}_m^{\text{BB}} \in \mathbb{C}^{N_{\text{Tx}}^{\text{RF}} \times 1}}} \|\mathbf{f}_m - \mathbf{F}_m^{\text{RF}} \mathbf{f}_m^{\text{BB}}\|_2 \quad (45)$$

for all  $m$ . If the least squares error is for all  $m$ , then the hybrid precoders  $\mathbf{F}_m^{\text{RF}} \mathbf{f}_m^{\text{BB}}$  perform as well as the digital ones  $\mathbf{f}_m$ . However, due to  $\mathbf{F}_m^{\text{RF}}$ , this is still a discrete optimization problem whose solution cannot be computed efficiently. Here, we improve on the approach proposed in [6], [33] based on compressive sensing tools by generalizing it to any type of array (not just ULAs) and by improving its performance.

Define the so-called dictionary matrix  $\mathbf{D}$  as the concatenation of all column vectors (atoms)  $\mathbf{d} \in \mathcal{X}^{N_{\text{Tx}} \times 1}$ . Then, problem (45) is equivalent to the following sparse recovery problem

$$\min_{\bar{\mathbf{f}}_m} \|\mathbf{f}_m - \mathbf{D} \bar{\mathbf{f}}_m\|_2 \quad (46a)$$

$$\text{s.t. } \|\bar{\mathbf{f}}_m\|_0 = N_{\text{Tx}}^{\text{RF}}, \quad (46b)$$

where  $\|\cdot\|_0$  denotes the pseudo- $\ell_0$ -norm. The output of problem (46a) is a  $N_{\text{Tx}}^{\text{RF}}$ -sparse vector  $\bar{\mathbf{f}}_m$ , whose non-zero entries correspond to the optimum  $\mathbf{f}_m^{\text{BB}}$  and whose support (indexes of the non-zero entries) point to the columns of  $\mathbf{D}$  which form the optimum matrix  $\mathbf{F}_m^{\text{RF}}$ . Due to the pseudo- $\ell_0$ -norm constraint (which is non-convex) problem (46a) still remains impractical. A fast suboptimal approach used in [6], [33] is to employ a greedy method such as orthogonal matching pursuit (OMP) [29]. Roughly speaking greedy methods construct the solution by finding the non-zero entries of  $\bar{\mathbf{f}}_m$  one at a time. The number of columns of  $\mathbf{D}$  grows exponentially with the number of antennas as  $Q^{N_{\text{Tx}}}$ , and therefore, so does the computational complexity and memory requirements of OMP [51]. In [6], [33], for the case of ULAs, the dictionary size problem is bypassed by appropriately choosing a small subset of columns; however, this approach is suboptimal and it is not easily generalized to arbitrary arrays.

The main idea of our approach is that the dictionary does not need to be explicitly computed during the execution of OMP, thus, avoiding the problems related to its size. The description of OMP is omitted as its detailed steps can be found in many works [29], [51], and instead focus on the single step that is computed differently. Briefly speaking, OMP is a recursive method, that at each iteration looks up the atom  $\mathbf{d}$  that correlates the most with the residue  $\mathbf{r}$  carried out from the previous iteration:  $\max_{\mathbf{d} \in \mathcal{X}^{N_{\text{Tx}} \times 1}} |\mathbf{d}^H \mathbf{r}| / \|\mathbf{d}\|$ . Using the fact that  $\|\mathbf{d}\| = \sqrt{N_{\text{Tx}}}$  because  $|d_i| = 1$  for any  $i$ , finding the best atom reduces to

$$\max_{\xi_1, \dots, \xi_{N_{\text{Tx}}}} \left| \sum_{i=1}^{N_{\text{Tx}}} e^{-j\xi_i} r_i \right|, \quad (47)$$

where we used the fact that  $d_i = e^{j\xi_i}$ , and it must belong to the set of discrete phases  $\xi_i \in \{0, 2\pi/Q, \dots, 2\pi(Q-1)/Q\}$  (43), for all  $i$ . Let  $\delta = 2\pi/2^{B_{\text{Tx}}}$  be the phase shifters resolution.

Upon defining  $v_i = e^{-j\xi_i} r_i$  for  $i = 1, \dots, N_{\text{Tx}}$ , step (47) can alternatively be expressed as

$$\max_{v_1, \dots, v_{N_{\text{Tx}}}} \left| \sum_{i=1}^{N_{\text{Tx}}} v_i \right| \quad (48)$$

subject to  $v_i = |r_i| e^{j(\angle r_i - \delta k_i)}$  for some integer  $k_i$  and for all  $i$ . Here,  $\angle$  denotes the phase of a complex number, and for convenience we define  $\angle 0 = 0$ . Note that if the optimal  $\{v_i\}_{i=1}^{N_{\text{Tx}}}$  are known, then the optimal phase shifts are  $\xi_i = \angle r_i - \angle v_i = \delta k_i$  for all  $i$ . The proposed method for solving (47) exploits the following lemma.

**Lemma 1.** *A solution to (47) is optimal only if*

$$|\angle v_i - \angle v_k|_{\text{wa}} \leq \delta \quad \text{for any } i, k. \quad (49)$$

Here,  $|\angle v_i - \angle v_k|_{\text{wa}}$  is the wrap-around phase difference, so that for  $\angle v_i = \frac{3\pi}{2}$  and  $\angle v_k = 0$ , the phase difference is  $\frac{\pi}{2}$  and not  $\frac{3\pi}{2}$ .

*Proof.* The proof is by contradiction. Let  $\{v_i\}_{i=1}^{N_{\text{Tx}}}$  be an optimum solution, and assume after reordering  $|\angle v_1 - \angle v_2|_{\text{wa}} > \delta$ . Define  $S = \sum_{i=3}^{N_{\text{Tx}}} v_i$  and further assume  $|\angle S - \angle v_1|_{\text{wa}} \leq |\angle S - \angle v_2|_{\text{wa}}$ . Then, it follows that  $|\angle(S+v_1) - \angle v_2|_{\text{wa}} > \delta/2$ . Note that if  $v_2$  is feasible, then  $v'_2 = v_2 e^{j\delta k'}$  for any integer  $k'$  is also a feasible point. By appropriately choosing  $k'$ ,  $v'_2$  is such that  $|\angle(S+v_1) - \angle v'_2|_{\text{wa}} \leq \delta/2$ . Since, the angle between  $S+v_1$  and  $v'_2$  is smaller than between  $S+v_1$  and  $v_2$ , it follows that  $|S+v_1+v_2| > |S+v_1+v'_2|$ , and consequently  $\{v_i\}_{i=1}^{N_{\text{Tx}}}$  cannot be optimum.  $\square$

Lemma 1 can be exploited to narrow the feasible set to very few choices because it states that all  $\{v_i\}$  must lie within a cone centered at the origin with an angular width of  $\delta$ , i.e.,

$$\psi \leq \angle v_i \leq \psi + \delta \quad (50)$$

for all  $i$  and some unknown  $\psi$ . For a given value of  $\psi$ , it exists only one feasible value of  $v_i$  satisfying (50) because its magnitude is prescribed  $|v_i| = |r_i|$  and its phase can be rotated multiples of  $\delta$  only (except if  $\angle r_i = \psi$  in which case  $\angle r_i = \psi + \delta$  is also feasible). Therefore, problem (48) boils down to performing a 1-dimensional search over  $\psi$  whose domain is  $[0, 2\pi)$ . Define  $v'_i = |v_i| e^{j(\angle v_i - \lfloor \psi \rfloor \delta)}$  where  $\lfloor \psi \rfloor \delta$  rounds  $\psi$  to the nearest multiple of  $\delta$  that is equal or smaller. Then, the search of  $\psi$  can be further reduced by noting that for a given  $\{v_i\}_{i=1}^{N_{\text{Tx}}}$  satisfying (50) for  $\delta \leq \psi < 2\pi$ , the alternate solution  $\{v'_i\}_{i=1}^{N_{\text{Tx}}}$  also satisfies (50) for  $0 \leq \psi < \delta$  and results in the same value of the objective function (48). Furthermore, since  $\angle v_i$  are constraint to phase shifts of the form  $\angle r_i - \delta k_i$ , for all  $i$ , the 1-dimensional search of  $\psi$  can be simplified to a few discrete phase shifts. With this in mind, we present Algorithm 2 for solving (47). Note that the actual value of  $\psi$  does not need to be explicitly computed.

Define a sector beam as a precoder having a large antenna gain within a certain range and low gain towards other directions. Fig. 4 shows a sector beam obtained with Algorithm 2 and that of [6]. Because the proposed method can compute (47) exactly, it is able to generate a proper sector beam with only 5 RF chains and 2-bit phase shifters, whereas the approach

---

**Algorithm 2** Optimal phase shifts (47)
 

---

**inputs:**  $r_1, \dots, r_{N_{\text{Tx}}}$  and  $\delta$   
**outputs:**  $\xi_1, \dots, \xi_{N_{\text{Tx}}}$

- 1: let  $\Omega(i)$  be a permutation such that  $0 \leq \text{mod}(\angle r_{\Omega(1)}, \delta) \leq \dots \leq \text{mod}(\angle r_{\Omega(N_{\text{Tx}})}, \delta) < \delta$
- 2: set  $x_i = |r_{\Omega(i)}| e^{j \text{mod}(\angle r_{\Omega(i)}, \delta)}$  for  $i = 1, \dots, N_{\text{Tx}}$
- 3: initialize  $S = 0$
- 4: **for**  $m = 1, \dots, N_{\text{Tx}}$  **do**
- 5:   **if**  $\left| \sum_{i=1}^{N_{\text{Tx}}} x_i \right| > S$  **then**
- 6:      $S = \left| \sum_{i=1}^{N_{\text{Tx}}} x_i \right|$
- 7:      $\xi_{\Omega(i)} = \angle r_{\Omega(i)} - \angle x_i$  for  $i = 1, \dots, N_{\text{Tx}}$
- 8:   **end if**
- 9:    $\angle x_m \leftarrow \angle x_m + \delta$
- 10: **end for**

---

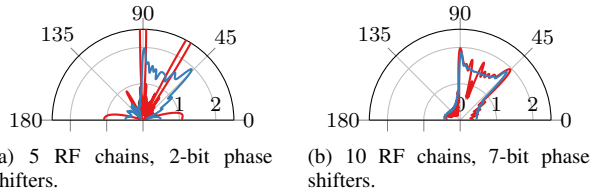


Fig. 4. In blue the proposed hybrid approximation. In red the approximation proposed by [6]. Only azimuth angles from  $0^\circ$  to  $180^\circ$  are plotted because the beampattern of a ULA is symmetric.

in [6] fails to achieve constant gain even with 10 RF chains and 7-bit phase shifters.

### C. Combiners Design

The Rx performs analog/RF combining and then applies digital signal processing to estimate the channel parameters. In Section IV-A, we observed that the received signal is projected onto a subspace of dimension  $N_{\text{Rx}}^{\text{RF}}$  spanned by  $\widetilde{\mathbf{W}}$ . Ideally, the analog combiners would be designed so that the received signal lies in the subspace spanned by the columns of  $\mathbf{W}$  for all possible AoAs/AoDs, in which case no information would be lost in the process; however this may not be possible. Thus, in this section, we propose to choose  $\mathbf{W}$  such that the average signal energy after projecting is maximized.

Assume all  $\phi \in \mathcal{R}_{\text{Rx}}$  are equally likely and  $\phi$  is independent of  $\theta$ . From (2) and (5), the average received energy as a function of  $\widetilde{\mathbf{W}}$  is proportional to

$$\mathbb{E}_{\phi, \theta} \text{SNR} \propto \mathbb{E}_{\phi, \theta} \left\| \widetilde{\mathbf{W}}^{\text{H}} \mathbf{a}_{\text{Rx}}(\phi) \mathbf{a}_{\text{Tx}}(\theta) \mathbf{F} \right\|_{\text{F}}^2 \quad (51)$$

$$\propto \int_{\mathcal{R}_{\text{Rx}}} \left\| \widetilde{\mathbf{W}}^{\text{H}} \mathbf{a}_{\text{Rx}}(\phi) \right\|_2^2 d\phi. \quad (52)$$

Employing grid (16), the integral can be approximated by a sum,

$$\mathbb{E}_{\phi, \theta} \text{SNR} \propto \sum_{q=1}^{S_{\text{Rx}}} \left\| \widetilde{\mathbf{W}}^{\text{H}} \mathbf{a}_{\text{Rx}}(\varphi^q) \right\|_2^2 \quad (53)$$

$$= \text{Tr} \widetilde{\mathbf{W}} \widetilde{\mathbf{W}}^{\text{H}} \mathbf{A}, \quad (54)$$

where  $\mathbf{A} = \sum_q \mathbf{a}_{\text{Rx}}(\varphi^q) \mathbf{a}_{\text{Rx}}^{\text{H}}(\varphi^q)$ . Let  $\lambda_1, \lambda_2, \dots$  be the eigenvalues of  $\mathbf{A}$  in non-increasing order. Then, according to majorization theory [44],  $\sum_{i=1}^{N_{\text{Rx}}^{\text{RF}}} \lambda_i$  is an upperbound on (54). This upperbound is achieved when the columns of  $\widetilde{\mathbf{W}}$  are the eigenvectors of  $\mathbf{A}$  associated to the  $N_{\text{Rx}}^{\text{RF}}$  largest eigenvalues; or equivalently, when the columns of  $\mathbf{W}$  span the same subspace. Unfortunately,  $\mathbf{W}$  cannot be chosen freely as its entries must belong to  $\mathcal{X}$  defined in (43). Thus, we propose an orthogonal matching pursuit approach for matrices (see Algorithm 3) suggested in [52]. A key aspect from this approach is that instead of computing  $\mathbf{W}$  directly, we estimate one column at a time.

---

**Algorithm 3** Computation of the analog combining matrix
 

---

**inputs:**  $\mathbf{A}, N_{\text{Rx}}^{\text{RF}}$   
**outputs:**  $\mathbf{W}$

- 1: initialize  $\mathbf{R} = \mathbf{A}$
- 2: **for**  $i = 1, \dots, N_{\text{Rx}}^{\text{RF}}$  **do**
- 3:   find the eigenvector  $\mathbf{u}$  of  $\mathbf{R}$  associated to the largest eigenvalue
- 4:   solve  $\max_{\mathbf{w}_i \in \mathcal{X}^{N_{\text{Rx}} \times 1}} |\mathbf{w}_i^{\text{H}} \mathbf{u}|$  with Algorithm 2
- 5:   update residue

$$\mathbf{R} = \left[ \mathbf{I}_{N_{\text{Rx}}} - \mathbf{B}_i (\mathbf{B}_i^{\text{H}} \mathbf{B}_i)^{-1} \mathbf{B}_i^{\text{H}} \right] \mathbf{A}$$

where  $\mathbf{B}_i = [\mathbf{w}_1, \dots, \mathbf{w}_i]$

- 6: **end for**
- 7:  $\mathbf{W} = [\mathbf{w}_1, \dots, \mathbf{w}_{N_{\text{Rx}}^{\text{RF}}}]$

---

In favor of the goodness of Algorithm 3 note that if the entries of  $\mathbf{W}$  are allowed to be arbitrary complex numbers, then Algorithm 3 outputs the optimum solution, i.e., the eigenvectors of  $\mathbf{A}$  associated to the  $N_{\text{Rx}}^{\text{RF}}$  largest eigenvalues. For the most efficient way to compute the residue in line 5 check [51].

## V. AOD AND AOA ESTIMATION BY 1-DIMENSIONAL SEARCH

In this section, the maximum likelihood estimator (MLE) of the AoD, AoA and channel gain are derived, altogether with low-complexity estimators approximations. Given the observations at the Rx (4),(5), the MLE is the maximizer of the likelihood function (66). By expanding the square of the norm and dropping terms that do not depend on the parameters, the MLE simplifies to

$$\arg \max_{\alpha, \theta, \phi} \left\{ |\alpha|^2 \left\| \widetilde{\mathbf{W}}^{\text{H}} \mathbf{a}_{\text{Rx}}(\phi) \right\|_2^2 \left\| \mathbf{F}^{\text{H}} \mathbf{a}_{\text{Tx}}(\theta) \right\|_2^2 - 2 \Re \alpha^* \mathbf{a}_{\text{Rx}}^{\text{H}}(\phi) \widetilde{\mathbf{W}} \widetilde{\mathbf{Y}} \mathbf{F}^{\text{H}} \mathbf{a}_{\text{Tx}}(\theta) \right\}, \quad (55)$$

where  $\Re$  denotes the real part. By taking the derivative with respect to  $\alpha$  and equating to zero, we find that the ML estimate of the channel gain for a given AoD and AoA is

$$\hat{\alpha} = \frac{\mathbf{a}_{\text{Rx}}^{\text{H}}(\phi) \widetilde{\mathbf{W}} \widetilde{\mathbf{Y}} \mathbf{F}^{\text{H}} \mathbf{a}_{\text{Tx}}(\theta)}{\left\| \widetilde{\mathbf{W}}^{\text{H}} \mathbf{a}_{\text{Rx}}(\phi) \right\|_2^2 \left\| \mathbf{F}^{\text{H}} \mathbf{a}_{\text{Tx}}(\theta) \right\|_2^2}. \quad (56)$$

Plugging  $\hat{\alpha}$  back to (55) and after simplification, the MLE on the AoD and AoA is reformulated as

$$\arg \max_{\theta, \phi} \frac{\left| \mathbf{a}_{\text{Rx}}^{\text{H}}(\phi) \widetilde{\mathbf{W}} \widetilde{\mathbf{Y}} \mathbf{F}^{\text{H}} \mathbf{a}_{\text{Tx}}(\theta) \right|^2}{\left\| \widetilde{\mathbf{W}}^{\text{H}} \mathbf{a}_{\text{Rx}}(\phi) \right\|_2^2 \left\| \mathbf{F}^{\text{H}} \mathbf{a}_{\text{Tx}}(\theta) \right\|_2^2}. \quad (57)$$

Thus, finding the ML estimates of the AoD and AoA requires performing a two-dimensional search, and thereafter the channel gain can be estimated in closed-form.

Next, we propose a suboptimal two-step approach with lower computational complexity. In the first step, the ML estimate of the received signals is obtained by taking into account that the signal part of the observations  $\widetilde{\mathbf{Y}}$  is rank 1 (due to  $\mathbf{H}$  being rank 1) and ignoring the knowledge on the array response function at the Tx and Rx, i.e.,

$$\min_{\mathbf{u}_l, \mu, \mathbf{u}_r} \left\| \widetilde{\mathbf{Y}} - \mathbf{u}_l \mu \mathbf{u}_r^{\text{H}} \right\|_{\text{F}}, \quad (58)$$

where we used the SVD to represent the rank 1 matrix estimate. According to the well known Eckart-Young-Mirsky theorem, (58) is minimized when  $\mu$  is the largest singular value of  $\widetilde{\mathbf{Y}}$ , and  $\mathbf{u}_l$  and  $\mathbf{u}_r$  are the corresponding left and right singular vectors, respectively. In the second step, we plug the estimated signal back to original MLE of the unknown parameters (57), resulting in

$$\arg \max_{\theta, \phi} \frac{\mu \left| \mathbf{u}_l^{\text{H}}(\phi) \widetilde{\mathbf{W}}^{\text{H}} \mathbf{a}_{\text{Rx}}(\phi) \right|^2 \left| \mathbf{u}_r^{\text{H}} \mathbf{F}^{\text{H}} \mathbf{a}_{\text{Tx}}(\theta) \right|^2}{\left\| \widetilde{\mathbf{W}}^{\text{H}} \mathbf{a}_{\text{Rx}}(\phi) \right\|_2^2 \left\| \mathbf{F}^{\text{H}} \mathbf{a}_{\text{Tx}}(\theta) \right\|_2^2}, \quad (59)$$

which decouples into two 1-dimensional searches,

$$\hat{\phi} = \arg \max_{\phi} \frac{\left| \mathbf{u}_l^{\text{H}} \widetilde{\mathbf{W}}^{\text{H}} \mathbf{a}_{\text{Rx}}(\phi) \right|^2}{\left\| \widetilde{\mathbf{W}}^{\text{H}} \mathbf{a}_{\text{Rx}}(\phi) \right\|_2^2} \quad (60)$$

$$\hat{\theta} = \arg \max_{\theta} \frac{\left| \mathbf{u}_r^{\text{H}} \mathbf{F}^{\text{H}} \mathbf{a}_{\text{Tx}}(\theta) \right|^2}{\left\| \mathbf{F}^{\text{H}} \mathbf{a}_{\text{Tx}}(\theta) \right\|_2^2}. \quad (61)$$

## VI. NUMERICAL RESULTS

The performance of the optimal robust precoders is illustrated by multiple Monte Carlo simulations. To this end, we define the following figures of merit which are in fact the objective functions of Problems 1–3, respectively,

$$\text{‘Worst case EB’} = \left( \max_{(\theta, \phi) \in \mathcal{R}_{\text{Tx}} \times \mathcal{R}_{\text{Rx}}} \text{EB} \right)^{\frac{1}{2}} \quad (62)$$

$$\text{‘Worst case DEB’} = \left( \max_{(\theta, \phi) \in \mathcal{R}_{\text{Tx}} \times \mathcal{R}_{\text{Rx}}} \text{DEB} \right)^{\frac{1}{2}} \quad (63)$$

$$\text{‘Worst case OEB’} = \left( \max_{(\theta, \phi) \in \mathcal{R}_{\text{Tx}} \times \mathcal{R}_{\text{Rx}}} \text{OEB} \right)^{\frac{1}{2}}, \quad (64)$$

where  $\text{EB} = \max\{\text{DEB}, \text{OEB}\}$ . For clarity, all of these metrics will be given in degrees and not radians. All numerical results are tested on 30-antenna ULAs or UCAs with an inter-antenna spacing of half wavelength. Unless otherwise stated, the Tx and Rx are equipped with hybrid arrays with 5 RF chains and 4-bit phase shifters. The SNR, as defined in (9), is set to  $-5$  dB. The number of training sequences transmitted is  $M = 5$ .

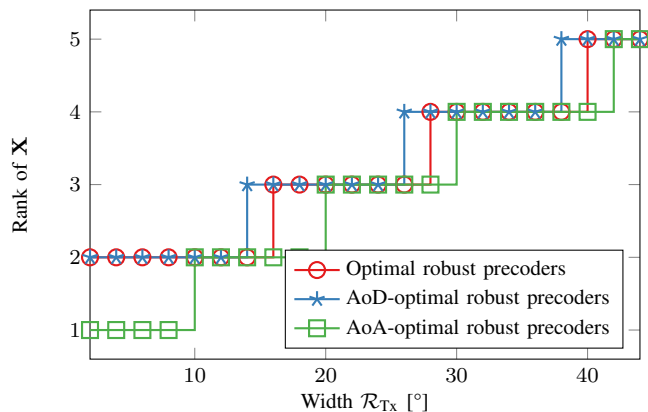


Fig. 5. Plot of the rank of matrix  $\mathbf{X}$  output by problem (25) vs. the a priori range  $\mathcal{R}_{\text{Tx}}$  width at the Tx. Parameter  $\rho$  which ensures that the AoDs are identifiable is set to  $\rho = 0.8$ .

### A. Analysis of the Optimality Condition C1

In Section III-B it was explained that a necessary condition for the optimality of the proposed precoders (in the sense that they are the solution to Problems 1 to 3) is that the condition  $M \geq \text{rank } \mathbf{X}$  is met, where  $M$  is the number of training sequences and  $\mathbf{X}$  is the solution to problem (25). Numerical evidence (see Fig. 5) suggests that the rank of  $\mathbf{X}$  increases with the width of  $\mathcal{R}_{\text{Tx}}$ , and while not shown here for space reasons, it also increases with the array aperture. Nonetheless, in general,  $\mathbf{X}$  is low rank, and therefore, only a few training sequences are required in order to ensure the optimality of the proposed precoders.

### B. Hybrid Precoders

In Section IV, methods for computing the hybrid precoders at the Tx and the analog combiners at the Rx were proposed. An important advantage of these methods compared to current approaches is that they rely on Algorithm 2 which is able to compute the optimal phase shifts efficiently. Fig. 6 compares the proposed approach for computing the hybrid precoders at the Tx compared to the approach proposed in [6], showcasing the vast improvement in performance. Notice, that with only 2-bit phase shifters and 3 RF chains, the proposed method achieves the same performance of a fully digital 30-antenna array. Conversely, the approach in [6] requires 6-bit phase shifters and 5 RF chains to match the same performance. For the latter approach, the cases with less than 5 bits have not been plotted because the EB is close to  $10^\circ$  and does not converge to the floor for any given number of RF chains.

Fig. 7 plots the performance achieved by Algorithm 3 in computing the analog weights at the Rx. To the best of the authors' knowledge, no other methods are known for computing these weights

### C. Estimators and Ambiguities

Let  $\hat{\theta}$  be an estimate on the AoD. Then, the worst case root mean square error (RMSE) on the AoD is defined as

$$\text{‘Worst case RMSE’} = \left( \max_{(\theta, \phi) \in \mathcal{R}_{\text{Tx}} \times \mathcal{R}_{\text{Rx}}} \mathbb{E} \left( \hat{\theta} - \theta \right)^2 \right)^{\frac{1}{2}}. \quad (65)$$

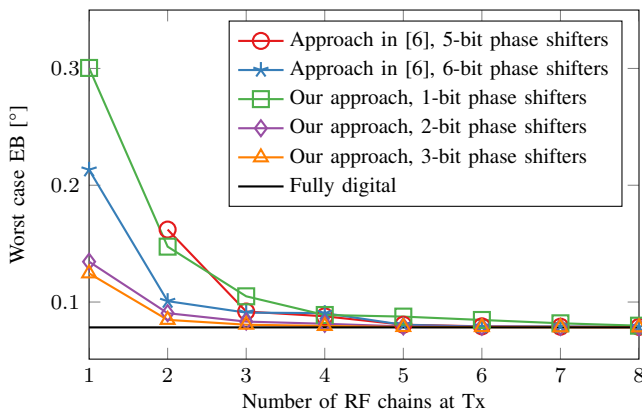


Fig. 6. Performance analysis of different hybrid precoding strategies. The Tx and Rx are equipped with a hybrid and fully digital ULA, respectively. The AoD (same for the AoA for simplicity) is known a priori to lie in the range  $[90^\circ, 100^\circ]$ .

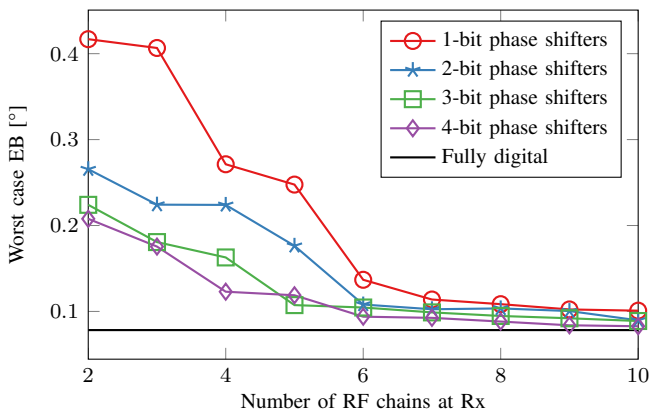


Fig. 7. Performance analysis of the proposed analog combiners at the Rx. The Tx and Rx are equipped with a fully digital and hybrid ULA, respectively. The AoD (same for the AoA for simplicity) is known a priori to lie in the range  $[90^\circ, 100^\circ]$ .

It can be easily verified that if the RMSE  $\mathbb{E}(\hat{\theta} - \theta)^2$  is tight to the DEB, such as is the case of the ML estimator, then the worst case RMSE is tight to the worst case DEB. Fig. 8 plots the worst case RMSE for the MLE and SOE (sub-optimal estimator) derived in Section V for different values of  $\rho$ . As expected, the MLE's worst case RMSE converges to the worst case DEB for a sufficient large SNR, and the SOE as well as its performance loss compared to the MLE is almost negligible. For decreasing values of  $\rho$ , the SNR threshold (which is the SNR value at which the estimators' accuracy matches the lower-bound) is shifted to the left. For  $\rho = 1$ , the identifiability constraint is removed and both estimators fail to correctly estimate the AoD for any given SNR.

#### D. Optimal Robust Precoders vs. Sector Beams

Most of the existing works on codebook design for mmWave channel estimation use the so-called sector beams [6], [8], [16], [21]. In such approaches the regions  $\mathcal{R}_{Tx}$  and/or  $\mathcal{R}_{Rx}$  are split evenly into  $M$  subregions. Ideally, each beam has maximum gain in one of these disjoint subregions and zero gain anywhere else. The main idea is that by detecting

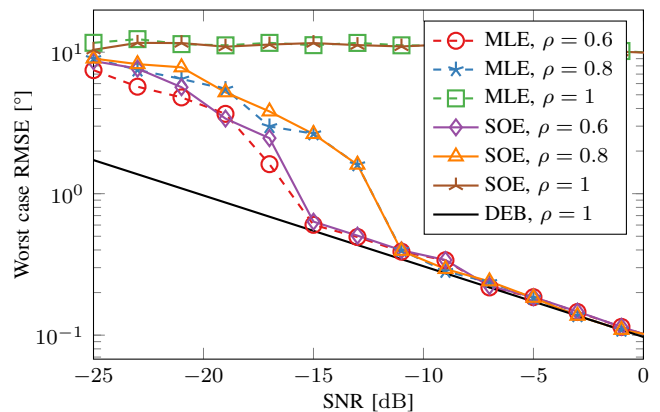


Fig. 8. AoD estimation accuracy vs. SNR for different values of  $\rho$  (defined in Section III-C1). Both, the Tx and the Rx, employ UCAs. The AoD (same for the AoA for simplicity) is known a priori to lie in the range  $[70^\circ, 90^\circ]$ .

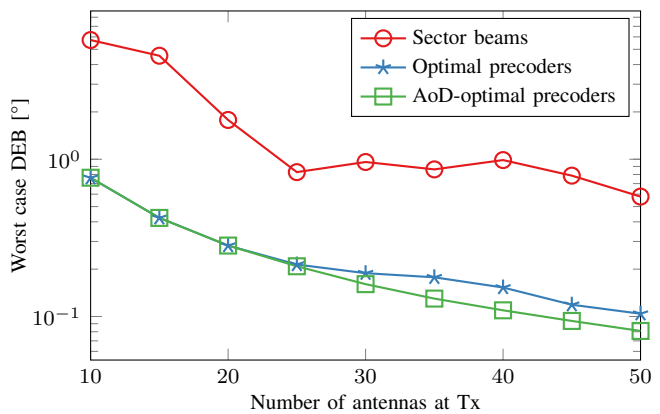


Fig. 9. Performance comparison between optimal robust precoders and sector beams. Both, the Tx and the Rx, are equipped with UCAs. The AoD (same for the AoA for simplicity) is known a priori to lie in the range  $[70^\circ, 90^\circ]$ .

the time instant leading to the largest power at the receiver, one can easily identify the transmitting and/or receiving beam, and therefore, the range of angles containing the AoD and/or AoA. Their use is widespread because they lead to simple AoD/AoA estimators and are intuitive, despite not necessary being optimal in the sense of minimizing the estimation error. Only approximate sector beams can be generated in practice because of the sharp discontinuities in the beam pattern.

Since the proposed approach in this paper keeps the combiners constant at the Rx throughout time, for a fair comparison, the sector beams are only generated at the Tx and the Rx is assumed to be a fully digital array. In this case, sector beams cannot estimate the AoA, thus, we analyze the performance of the proposed optimal robust precoders and the sector beams only in terms of AoD estimation, i.e., in terms of DEB. Fig 9 plots the worst case DEB for both methodologies. The sector beams are designed with the procedure in [6]. Note that the optimal robust precoders outperform the sector beams by almost an order of magnitude.

## VII. CONCLUSIONS

We proposed a method for computing the optimal robust precoders for estimating the channel when a priori knowledge

on the AoD/AoA is available. Simulations revealed that the estimation accuracy of the proposed beams is remarkably superior to the more common sector beams. The computation of the optimal precoders is achieved by solving a conic optimization problem which may be too computationally intensive for real-time application, thus faster algorithms need to be developed in this regard. Nonetheless, the proposed precoders may be useful for benchmarking purposes as they minimize the worst case CRB on the AoD/AoA. Contrary to previous works which used a suboptimal approximation of OMP to compute the precoders for hybrid architectures, an efficient method for applying OMP has been provided. The resulting hybrid precoders using exact OMP matched the performance of the digital precoders on a 30-antenna arrays with only 2-bit phase shifters and 3 RF chains. Moreover, we have shown that performing digital combining is suboptimal when performing channel estimation, and instead, we should strike for analog combining only, and then apply digital signal processing to estimate the parameters. To this end, an algorithm for designing the analog combiners has been provided. To verify that the lower-bounds used in the design of the precoders are tight, we have derived the ML estimator (and also a low-complex variation) on the AoD, AoA and channel gain, and verified numerically that the MLE's variance converges to the lower bound for average to high SNR.

#### APPENDIX

Assume perfect time synchronization, then the log-likelihood function of the observations (4) is proportional to

$$\log \rho(\mathbf{Y}|\theta, \phi, \alpha) \propto \frac{1}{\sigma^2} \left\| \tilde{\mathbf{Y}} - \|\mathbf{s}\|_2 \tilde{\mathbf{W}}^H \mathbf{H} \mathbf{F} \right\|_F^2, \quad (66)$$

where  $\tilde{\mathbf{Y}} = (\mathbf{W}^H \mathbf{W})^{-\frac{1}{2}} \mathbf{Y}$  and  $\mathbf{H}$ , defined in (2), depends on the unknown parameters. According to the analysis of [23], the Fisher information matrix of the unknown parameters turns out to be

$$\mathbf{J} = \begin{bmatrix} \Phi_{\theta, \theta} & \Phi_{\theta, \phi} & \Phi_{\theta, \Re\alpha} & \Phi_{\theta, \Im\alpha} \\ \Phi_{\theta, \phi} & \Phi_{\phi, \phi} & \Phi_{\phi, \Re\alpha} & \Phi_{\phi, \Im\alpha} \\ \Phi_{\theta, \Re\alpha} & \Phi_{\phi, \Re\alpha} & \Phi_{\Re\alpha, \Re\alpha} & 0 \\ \Phi_{\theta, \Im\alpha} & \Phi_{\phi, \Im\alpha} & 0 & \Phi_{\Im\alpha, \Im\alpha} \end{bmatrix}, \quad (67)$$

where<sup>4</sup>

$$\Phi_{\theta, \theta} = \frac{2|\alpha|^2}{\sigma^2} \|\tilde{\mathbf{a}}_{\text{Rx}}(\phi)\|_2^2 \left\| \dot{\tilde{\mathbf{a}}}_{\text{Tx}}(\theta) \right\|_2^2 \quad (68a)$$

$$\Phi_{\theta, \phi} = \frac{2|\alpha|^2}{\sigma^2} \left\| \dot{\tilde{\mathbf{a}}}_{\text{Rx}}(\phi) \right\|_2^2 \|\tilde{\mathbf{a}}_{\text{Tx}}(\theta)\|_2^2 \quad (68b)$$

$$\Phi_{\Re\alpha, \Re\alpha} = \Phi_{\Im\alpha, \Im\alpha} = \frac{2}{\sigma^2} \|\tilde{\mathbf{a}}_{\text{Rx}}(\phi)\|_2^2 \|\tilde{\mathbf{a}}_{\text{Tx}}(\theta)\|_2^2 \quad (68c)$$

$$\Phi_{\theta, \phi} = \frac{2|\alpha|^2}{\sigma^2} \Re \left[ \tilde{\mathbf{a}}_{\text{Rx}}^H(\phi) \dot{\tilde{\mathbf{a}}}_{\text{Rx}}(\phi) \tilde{\mathbf{a}}_{\text{Tx}}^H(\theta) \dot{\tilde{\mathbf{a}}}_{\text{Tx}}(\theta) \right] \quad (68d)$$

$$\Phi_{\theta, \Re\alpha} = \frac{2}{\sigma^2} \|\tilde{\mathbf{a}}_{\text{Rx}}(\phi)\|_2^2 \Re \left[ \alpha \dot{\tilde{\mathbf{a}}}_{\text{Tx}}^H(\theta) \tilde{\mathbf{a}}_{\text{Tx}}(\theta) \right] \quad (68e)$$

$$\Phi_{\theta, \Im\alpha} = \frac{2}{\sigma^2} \|\tilde{\mathbf{a}}_{\text{Rx}}(\phi)\|_2^2 \Im \left[ \alpha \dot{\tilde{\mathbf{a}}}_{\text{Tx}}^H(\theta) \tilde{\mathbf{a}}_{\text{Tx}}(\theta) \right] \quad (68f)$$

$$\Phi_{\phi, \Re\alpha} = \frac{2}{\sigma^2} \Re \left[ \alpha \tilde{\mathbf{a}}_{\text{Rx}}^H(\phi) \dot{\tilde{\mathbf{a}}}_{\text{Rx}}(\phi) \right] \|\tilde{\mathbf{a}}_{\text{Tx}}(\theta)\|_2^2 \quad (68g)$$

<sup>4</sup>Contrary to [23], we have not assumed that  $\|\mathbf{a}_{\text{Tx}}(\theta)\| = \|\mathbf{a}_{\text{Rx}}(\phi)\| = 1$ .

$$\Phi_{\phi, \Im\alpha} = \frac{2}{\sigma^2} \Im \left[ \alpha \tilde{\mathbf{a}}_{\text{Rx}}^H(\phi) \dot{\tilde{\mathbf{a}}}_{\text{Rx}}(\phi) \right] \|\tilde{\mathbf{a}}_{\text{Tx}}(\theta)\|_2^2, \quad (68h)$$

$\tilde{\mathbf{a}}_{\text{Rx}}(\phi) \triangleq \tilde{\mathbf{W}}^H \mathbf{a}_{\text{Rx}}(\phi)$ ,  $\dot{\tilde{\mathbf{a}}}_{\text{Rx}}(\phi) \triangleq \frac{d}{d\phi} \tilde{\mathbf{W}}^H \mathbf{a}_{\text{Rx}}(\phi)$ ,  $\tilde{\mathbf{a}}_{\text{Tx}}(\theta) \triangleq \mathbf{F}^H \mathbf{a}_{\text{Tx}}(\theta)$  and  $\dot{\tilde{\mathbf{a}}}_{\text{Tx}}(\theta) \triangleq \frac{d}{d\theta} \mathbf{F}^H \mathbf{a}_{\text{Tx}}(\theta)$ . The CRB requires inverting the FIM. Define

$$\mathbf{J}_{11} = \begin{bmatrix} \Phi_{\theta, \theta} & \Phi_{\theta, \phi} \\ \Phi_{\phi, \theta} & \Phi_{\phi, \phi} \end{bmatrix} \quad (69)$$

$$\mathbf{J}_{12} = \mathbf{J}_{21}^T = \begin{bmatrix} \Phi_{\theta, \Re\alpha} & \Phi_{\theta, \Im\alpha} \\ \Phi_{\phi, \Re\alpha} & \Phi_{\phi, \Im\alpha} \end{bmatrix} \quad (70)$$

$$\mathbf{J}_{22} = \begin{bmatrix} \Phi_{\Re\alpha, \Re\alpha} & 0 \\ 0 & \Phi_{\Im\alpha, \Im\alpha} \end{bmatrix}. \quad (71)$$

Then, by the block matrix inversion formula, the CRB on the AoD and AoA is

$$(\mathbf{J}_{11} - \mathbf{J}_{12} \mathbf{J}_{22}^{-1} \mathbf{J}_{21})^{-1} = \begin{bmatrix} \text{DEB} & 0 \\ 0 & \text{OEB} \end{bmatrix} \quad (72)$$

where

$$\text{DEB}^{-1} = \frac{2|\alpha|^2}{\sigma^2} \|\tilde{\mathbf{a}}_{\text{Rx}}(\phi)\|_2^2 \left( \left\| \dot{\tilde{\mathbf{a}}}_{\text{Tx}}(\theta) \right\|_2^2 - \frac{|\tilde{\mathbf{a}}_{\text{Tx}}^H(\theta) \dot{\tilde{\mathbf{a}}}_{\text{Tx}}(\theta)|^2}{\|\tilde{\mathbf{a}}_{\text{Tx}}(\theta)\|_2^2} \right) \quad (73)$$

$$\text{OEB}^{-1} = \frac{2|\alpha|^2}{\sigma^2} \|\tilde{\mathbf{a}}_{\text{Tx}}(\theta)\|_2^2 \left( \left\| \dot{\tilde{\mathbf{a}}}_{\text{Rx}}(\phi) \right\|_2^2 - \frac{|\tilde{\mathbf{a}}_{\text{Rx}}^H(\phi) \dot{\tilde{\mathbf{a}}}_{\text{Rx}}(\phi)|^2}{\|\tilde{\mathbf{a}}_{\text{Rx}}(\phi)\|_2^2} \right). \quad (74)$$

#### REFERENCES

- [1] W. Roh, J.-Y. Seol, J. Park, B. Lee, J. Lee, Y. Kim, J. Cho, K. Cheun, and F. Aryanfar, "Millimeter-wave beamforming as an enabling technology for 5G cellular communications: theoretical feasibility and prototype results," *IEEE Communications Magazine*, vol. 52, no. 2, pp. 106–113, 2014.
- [2] P. Wang, Y. Li, L. Song, and B. Vucetic, "Multi-gigabit millimeter wave wireless communications for 5G: From fixed access to cellular networks," *IEEE Communications Magazine*, vol. 53, no. 1, pp. 168–178, 2015.
- [3] S. Kutty and D. Sen, "Beamforming for millimeter wave communications: An inclusive survey," *IEEE Communications Surveys & Tutorials*, vol. 18, no. 2, pp. 949–973, 2016.
- [4] T. S. Rappaport, G. R. MacCartney, M. K. Samimi, and S. Sun, "Wideband millimeter-wave propagation measurements and channel models for future wireless communication system design," *IEEE Transactions on Communications*, vol. 63, no. 9, pp. 3029–3056, 2015.
- [5] W. Keusgen, R. J. Weiler, M. Peter, M. Wisotzki, and B. Göktepe, "Propagation measurements and simulations for millimeter-wave mobile access in a busy urban environment," in *39th International Conference on Infrared, Millimeter, and Terahertz waves*. IEEE, 2014, pp. 1–3.
- [6] A. Alkhateeb, O. El Ayach, G. Leus, and R. W. Heath, "Channel estimation and hybrid precoding for millimeter wave cellular systems," *IEEE Journal of Selected Topics in Signal Processing*, vol. 8, no. 5, pp. 831–846, 2014.
- [7] T. E. Bogale, L. B. Le, and X. Wang, "Hybrid analog-digital channel estimation and beamforming: Training-throughput tradeoff," *IEEE Transactions on Communications*, vol. 63, no. 12, pp. 5235–5249, 2015.
- [8] Z. Xiao, T. He, P. Xia, and X.-G. Xia, "Hierarchical codebook design for beamforming training in millimeter-wave communication," *IEEE Transactions on Wireless Communications*, vol. 15, no. 5, pp. 3380–3392, 2016.
- [9] K. Venugopal, A. Alkhateeb, N. G. Prelcic, and R. W. Heath Jr, "Channel estimation for hybrid architecture based wideband millimeter wave systems," *arXiv preprint arXiv:1611.03046*, 2016.
- [10] J. Rodríguez-Fernández, N. González-Prelcic, and R. W. Heath, "Channel estimation in mixed hybrid-low resolution MIMO architectures for mmWave communication," in *Signals, Systems and Computers, 2016 50th Asilomar Conference on*. IEEE, 2016, pp. 768–773.
- [11] V. Va, T. Shimizu, G. Bansal, R. W. Heath Jr *et al.*, "Millimeter wave vehicular communications: A survey," *Foundations and Trends® in Networking*, vol. 10, no. 1, pp. 1–113, 2016.

- [12] J. Choi, V. Va, N. González-Prelcic, R. Daniels, C. R. Bhat, and R. W. Heath Jr, "Millimeter wave vehicular communication to support massive automotive sensing," *IEEE Communications Magazine*, vol. 54, no. 12, pp. 160–167, 2016.
- [13] P. Sanchis, J. Martinez, J. Herrera, V. Polo, J. Corral, and J. Marti, "A novel simultaneous tracking and direction of arrival estimation algorithm for beam-switched base station antennas in millimeter-wave wireless broadband access networks," in *IEEE Antennas and Propagation Society International Symposium*, vol. 1, 2002, pp. 594–597.
- [14] J. Seo, Y. Sung, G. Lee, and D. Kim, "Training beam sequence design for millimeter-wave MIMO systems: A POMDP framework," *submitted for publication*, 2015.
- [15] J. He, T. Kim, H. Ghauch, K. Liu, and G. Wang, "Millimeter wave MIMO channel tracking systems," in *Globecom Workshops*. IEEE, 2014, pp. 416–421.
- [16] M. Kokshoorn, P. Wang, Y. Li, and B. Vucetic, "Fast channel estimation for millimetre wave wireless systems using overlapped beam patterns," in *IEEE International Conference on Communications (ICC)*, 2015, pp. 1304–1309.
- [17] R. Di Taranto, S. Muppirisetty, R. Raulefs, D. Slock, T. Svensson, and H. Wymeersch, "Location-aware communications for 5G networks: How location information can improve scalability, latency, and robustness of 5G," *IEEE Signal Processing Magazine*, vol. 31, no. 6, pp. 102–112, 2014.
- [18] V. Va, T. Shimizu, G. Bansal, and R. W. Heath, "Beam design for beam switching based millimeter wave vehicle-to-infrastructure communications," in *International Conference on Communications*. IEEE, 2016, pp. 1–6.
- [19] N. Garcia, H. Wymeersch, E. G. Ström, and D. Slock, "Location-aided mm-wave channel estimation for vehicular communication," in *17th International Workshop on Signal Processing Advances in Wireless Communications*. IEEE, 2016, pp. 1–5.
- [20] T. Nitsche, C. Cordeiro, A. B. Flores, E. W. Knightly, E. Perahia, and J. C. Widmer, "IEEE 802.11 ad: directional 60 Ghz communication for multi-Gigabit-per-second wi-fi," *IEEE Communications Magazine*, vol. 52, no. 12, pp. 132–141, 2014.
- [21] J. Wang, Z. Lan, C.-S. Sum, C.-W. Pyo, J. Gao, T. Baykas, A. Rahman, R. Funada, F. Kojima, I. Lakkis *et al.*, "Beamforming codebook design and performance evaluation for 60GHz wideband WPANs," in *IEEE 70th Vehicular Technology Conference Fall*, 2009, pp. 1–6.
- [22] T. S. Rappaport, S. Sun, R. Mayzus, H. Zhao, Y. Azar, K. Wang, G. N. Wong, J. K. Schulz, M. Samimi, and F. Gutierrez, "Millimeter wave mobile communications for 5G cellular: It will work!" *IEEE Access*, vol. 1, pp. 335–349, May 2013.
- [23] A. Shahmansoori, G. E. Garcia, G. Destino, G. Seco-Granados, and H. Wymeersch, "5G position and orientation estimation through millimeter wave MIMO," in *GLOBECOM 2015*. IEEE, 2015, pp. 1–6.
- [24] H. Wymeersch, G. Seco-Granados, G. Destino, D. Dardari, and F. Tufvesson, "5G mm-Wave positioning for vehicular networks," *IEEE Wireless Communications Magazine*, in press.
- [25] Y. Yu, P. G. Baltus, A. de Graauw, E. van der Heijden, C. S. Vaucher, and A. H. van Roermund, "A 60 Ghz phase shifter integrated with LNA and PA in 65 nm CMOS for phased array systems," *IEEE Journal of Solid-State Circuits*, vol. 45, no. 9, pp. 1697–1709, 2010.
- [26] R. Méndez-Rial, C. Rusu, N. González-Prelcic, A. Alkhateeb, and R. W. Heath, "Hybrid mimo architectures for millimeter wave communications: Phase shifters or switches?" *IEEE Access*, vol. 4, pp. 247–267, 2016.
- [27] S. Jacobsson, G. Durisi, M. Coldrey, U. Gustavsson, and C. Studer, "One-bit massive MIMO: Channel estimation and high-order modulations," in *International Conference on Communication Workshop*. IEEE, 2015, pp. 1304–1309.
- [28] J. Brady, N. Behdad, and A. M. Sayeed, "Beamspace MIMO for millimeter-wave communications: System architecture, modeling, analysis, and measurements," *IEEE Transactions on Antennas and Propagation*, vol. 61, no. 7, pp. 3814–3827, 2013.
- [29] Y. C. Pati, R. Rezaifar, and P. Krishnaprasad, "Orthogonal matching pursuit: Recursive function approximation with applications to wavelet decomposition," in *27th Asilomar Conference on Signals, Systems and Computers*. IEEE, 1993, pp. 40–44.
- [30] V. Venkateswaran and A.-J. van der Veen, "Analog beamforming in MIMO communications with phase shift networks and online channel estimation," *IEEE Transactions on Signal Processing*, vol. 58, no. 8, pp. 4131–4143, 2010.
- [31] D. De Donno, J. P. Beltrán, D. Giustiniano, and J. Widmer, "Hybrid analog-digital beam training for mmWave systems with low-resolution RF phase shifters," in *IEEE International Conference on Communications Workshops*, 2016, pp. 700–705.
- [32] J. Mirza, B. Ali, S. S. Naqvi, and S. Saleem, "Hybrid precoding via successive refinement for millimeter wave MIMO communication systems," *IEEE Communications Letters*, 2017.
- [33] O. El Ayach, R. W. Heath, S. Abu-Surra, S. Rajagopal, and Z. Pi, "Low complexity precoding for large millimeter wave mimo systems," in *Communications (ICC), 2012 IEEE International Conference on*. IEEE, 2012, pp. 3724–3729.
- [34] A. Alkhateeb, O. El Ayach, G. Leus, and R. W. Heath, "Hybrid precoding for millimeter wave cellular systems with partial channel knowledge," in *IEEE Information Theory and Applications Workshop*, 2013, pp. 1–5.
- [35] H. L. Van Trees, *Detection, estimation, and modulation theory*. John Wiley & Sons, 2004.
- [36] M. S. Lobo, L. Vandenberghe, S. Boyd, and H. Lebret, "Applications of second-order cone programming," *Linear algebra and its applications*, vol. 284, no. 1, pp. 193–228, 1998.
- [37] S. Boyd and L. Vandenberghe, *Convex optimization*. Cambridge university press, 2004.
- [38] M. Grant, S. Boyd, and Y. Ye, "CVX: Matlab software for disciplined convex programming," 2008.
- [39] MOSEK ApS, "The MOSEK optimization toolbox for MATLAB manual, version 7.1 (revision 51)," <http://mosek.com>, (accessed on March 20, 2016).
- [40] E. Bashan, A. J. Weiss, and B.-S. Yaakov, "Estimation near "zero information" points: angle-of-arrival near the endfire," *IEEE Transactions on Aerospace and Electronic Systems*, vol. 43, no. 4, pp. 1250–1264, 2007.
- [41] P. Stoica and A. Nehorai, "MUSIC, maximum likelihood, and Cramer-Rao bound," *IEEE Transactions on Acoustics, Speech, and Signal Processing*, vol. 37, no. 5, pp. 720–741, 1989.
- [42] B. Recht, M. Fazel, and P. A. Parrilo, "Guaranteed minimum-rank solutions of linear matrix equations via nuclear norm minimization," *SIAM review*, vol. 52, no. 3, pp. 471–501, 2010.
- [43] M. Fazel, H. Hindi, and S. P. Boyd, "A rank minimization heuristic with application to minimum order system approximation," in *American Control Conference, 2001*, vol. 6. IEEE, 2001, pp. 4734–4739.
- [44] I. Olkin and A. W. Marshall, *Inequalities: theory of majorization and its applications*. Academic press, 1979, vol. 143.
- [45] R. B. Bendel and M. R. Mickey, "Population correlation matrices for sampling experiments," *Communications in Statistics-Simulation and Computation*, vol. 7, no. 2, pp. 163–182, 1978.
- [46] P. I. Davies and N. J. Higham, "Numerically stable generation of correlation matrices and their factors," *BIT Numerical Mathematics*, vol. 40, no. 4, pp. 640–651, 2000.
- [47] I. S. Dhillon, R. W. Heath Jr, M. A. Sustik, and J. A. Tropp, "Generalized finite algorithms for constructing hermitian matrices with prescribed diagonal and spectrum," *SIAM Journal on Matrix Analysis and Applications*, vol. 27, no. 1, pp. 61–71, 2005.
- [48] H.-H. Lee and Y.-C. Ko, "Low complexity codebook-based beamforming for MIMO-OFDM systems in millimeter-wave WPAN," *IEEE Transactions on Wireless Communications*, vol. 10, no. 11, pp. 3607–3612, 2011.
- [49] L. C. Godara and A. Cantoni, "Uniqueness and linear independence of steering vectors in array space," *The Journal of the Acoustical Society of America*, vol. 70, no. 2, pp. 467–475, 1981.
- [50] H. Gazzah and K. Abed-Meraim, "Optimum ambiguity-free directional and omnidirectional planar antenna arrays for DOA estimation," *IEEE Transactions on signal processing*, vol. 57, no. 10, pp. 3942–3953, 2009.
- [51] B. L. Sturm, M. Grösch *et al.*, "Comparison of orthogonal matching pursuit implementations," in *20th European Signal Processing Conference (EUSIPCO)*. IEEE, 2012, pp. 220–224.
- [52] K. Lee and Y. Bresler, "ADMIRA: Atomic decomposition for minimum rank approximation," *IEEE Transactions on Information Theory*, vol. 56, no. 9, pp. 4402–4416, 2010.